MOUNTAIN-PLAINS CONSORTIUM

MPC 16-307 | R. Schmidt

Structural Health Monitoring of Highway Bridges Subjected to Overweight Trucks, Phase I – Instrumentation Development and Validation

MPC
MOUNTAIN-PLAINS CONSORTIUM

A University Transportation Center sponsored by the U.S. Department of Transportation serving the Mountain-Plains Region. Consortium members:

Colorado State University
North Dakota State University
South Dakota State University
University of Colorado Denver
University of Denver
University of Utah
Utah State University
University of Wyoming

Structural Health Monitoring of Highway Bridges Subjected to Overweight Trucks, Phase I – Instrumentation Development and Validation

Richard J. Schmidt
ORCID number 0000-0003-1672-2625
Department of Civil and Architectural Engineering
University of Wyoming
Laramie, Wyoming 82071

March 2016

Forward

Purpose of the Report: This document is the final report of research sponsored by the Federal Highway Administration, the Wyoming Department of Transportation, and the Mountain Plains Consortium.
Content Summary: This report contains the results of Phase I of a research project intended to develop a structural health monitoring system for highway bridges using fiber Bragg gratings as the strain sensors. The objectives are to provide long-term sensing of bridges that are subjected to overweight and other permit vehicles such that the accuracy of bridge rating software can be evaluated.
Interested Audience: Bridge owners and operators, bridge maintenance personnel, individuals interested in structural health monitoring of bridges
Previous Printings of the Publication: none
Publication Status: Final

Disclaimer Notice

Quality Assurance Statement

The Federal Highway Administration (FHWA) provides high-quality information to serve government, industry, and the public in a manner that promotes public understanding. Standards and policies are used to ensure and maximize the quality, objectivity, utility, and integrity of its information. FHWA periodically reviews quality issues and adjusts its programs and processes to ensure continuous quality improvement.

Acknowledgements

This report is based largely on the research and master's theses by University of Wyoming graduate students Mr. Danial Maurais, Mr. Michael Jung, and Ms. McKenzie Danforth. The invaluable contributions of Mr. James Branscomb to development of the microprocessor controllers for this study are also acknowledged.

Metric Conversion Chart

SI* (MODERN METRIC) CONVERSION FACTORS

APPROXIMATE CONVERSIONS TO SI UNITS

Symbol	When You Know	Multiply By	To Find	Symbol
		LENGTH		
in	inches	25.4	millimeters	mm
ft	feet	0.305	meters	m
yd	yards	0.914	meters	m
mi	miles	1.61	kilometers	km
		AREA		
in^2	square inches	645.2	square millimeters	mm^2
ft^2	square feet	0.093	square meters	m^2
yd^2	square yard	0.836	square meters	m^2
ac	acres	0.405	hectares	ha
mi^2	square miles	2.59	square kilometers	km^2
		VOLUME		
fl oz	fluid ounces	29.57	milliliters	mL
gal	gallons	3.785	liters	L
ft^3	cubic feet	0.028	cubic meters	m^3
yd^3	cubic yards	0.765	cubic meters	m^3
	NOTE: volumes greater than 1000 L shall be shown in m^3			
		MASS		
oz	ounces	28.35	grams	g
lb	pounds	0.454	kilograms	kg
T	short tons (2000 lb)	0.907	megagrams (or "metric ton")	Mg (or "t")
		TEMPERATURE (exact degrees)		
°F	Fahrenheit	5 (F-32)/9 or (F-32)/1.8	Celsius	°C
		ILLUMINATION		
fc	foot-candles	10.76	lux	lx
fl	foot-Lamberts	3.426	$candela/m^2$	cd/m^2
		FORCE and PRESSURE or STRESS		
lbf	poundforce	4.45	newtons	N
lbf/in^2	poundforce per square inch	6.89	kilopascals	kPa

APPROXIMATE CONVERSIONS FROM SI UNITS

Symbol	When You Know	Multiply By	To Find	Symbol
		LENGTH		
mm	millimeters	0.039	inches	in
m	meters	3.28	feet	ft
m	meters	1.09	yards	yd
km	kilometers	0.621	miles	mi
		AREA		
mm^2	square millimeters	0.0016	square inches	in^2
m^2	square meters	10.764	square feet	ft^2
m^2	square meters	1.195	square yards	yd^2
ha	hectares	2.47	acres	ac
km^2	square kilometers	0.386	square miles	mi^2
		VOLUME		
mL	milliliters	0.034	fluid ounces	fl oz
L	liters	0.264	gallons	gal
m^3	cubic meters	35.314	cubic feet	ft^3
m^3	cubic meters	1.307	cubic yards	yd^3
		MASS		
g	grams	0.035	ounces	oz
kg	kilograms	2.202	pounds	lb
Mg (or "t")	megagrams (or "metric ton")	1.103	short tons (2000 lb)	T
		TEMPERATURE (exact degrees)		
°C	Celsius	1.8C+32	Fahrenheit	°F
		ILLUMINATION		
lx	lux	0.0929	foot-candles	fc
cd/m^2	$candela/m^2$	0.2919	foot-Lamberts	fl
		FORCE and PRESSURE or STRESS		
N	newtons	0.225	poundforce	lbf
kPa	kilopascals	0.145	poundforce per square inch	lbf/in^2

*SI is the symbol for the International System of Units. Appropriate rounding should be made to comply with Section 4 of ASTM E380.
(Revised March 2003)

TABLE OF CONTENTS

LIST OF FIGURES

1. EXECUTIVE SUMMARY

1.1 Purpose of the Study

State departments of transportation (DOTs) in the west have been under increasing pressure to permit and route overweight trucks transporting machinery and equipment for the energy sector through their state and interstate highway systems. DOT engineers are called upon daily to rate their bridges for overweight trucks to determine appropriate truck routing and to assess the impacts of the trucks on bridge safety and durability. Many of these overweight trucks have nonstandard configurations, which further complicates the rating and permitting process. Hence, it is critical that bridge engineers in the DOTs develop confidence that their bridge analysis and rating software accurately predicts the response of bridges to overweight trucks, especially for bridges on the most frequently traveled routes.

The long-term objectives of this project were to develop and validate an instrumentation package for structural health monitoring (SHM) of bridges subjected to overweight trucks and to develop plans for field deployment of the instrumentation on a pilot scale. Ultimately, the objective is to accurately correlate long-term field performance data to the behavior of the bridges predicted by analysis and rating software. The field instrumentation package incorporates use of optical fiber sensors, specifically fiber Bragg gratings (FBGs), to monitor strains at critical locations in bridges that are considered most vulnerable to overweight truck loads and are most difficult to effectively rate with currently used software.

1.2 General Approach

In Phase I of the project, instrumentation, packaging, installation techniques, and data acquisition for fiber Bragg grating (FBG) sensors were be developed in the laboratory. The laboratory investigation included the following primary tasks:

1. Development of optical-fiber packaging or other protection mechanisms suitable for installation in the target environments, including both steel and concrete girder bridges.
2. Development of a low-cost, compact, and energy-efficient instrumentation package for interrogating the sensor network. The approach involved a combination of design and fabrication of custom instrumentation linked to commercially available components with proven reliability.
3. Development of data collection, processing, and transmission capabilities for an FBG sensor network on a bridge.
4. Validation of tasks 1, 2, and 3 in the laboratory using a mock-up of bridges having steel and concrete girders.
5. Determine if micro-buckling of FBG sensors strained in compression occurs and the means that can be employed to prevent it, thus allowing the sensors to accurately respond to compressive strain.

1.3 Findings and Conclusions

1.3.1 Task 1

FBG Sensors Mounted on Concrete

Both experimental and finite element methods were used to determine the elasto-mechanical behavior of FBG sensors attached to a concrete host. The conclusions drawn from the finite element analysis (FEA) and the experimental tests relate primarily to the strain measurement accuracy of the FBG sensors bonded

to concrete in notches. It was found that the FEA slightly over-predicts the strain transfer to the FBG when compared to test results. This conclusion is supported by the fact that for 80% of the configurations that were compared, the FEA strain transfer results were 1% to 9% greater than those seen in the experimental tests. Despite the FEA over-prediction, it is still possible to conclude there are some configurations that provide full strain transfer and some that do not.

After several laboratory and computer simulations of the FBG embedment procedure, it was concluded that the equipment and materials required to install an FBG in a notched concrete structural member are effective and obtainable for an engineering or construction crew. The embedment notches can be cut in the concrete with a masonry saw or formed as the concrete is placed. The Ultrabond 1300 epoxy was effective because of its short cure time and availability; however, for overhead or vertical applications, a more paste-like adhesive with higher viscosity would be optimal.

The FEA results supported several conclusions about how the configuration parameters affect the strain transfer for the notch-embedment sensing method. One undeniable conclusion is that as epoxy bond length increases, so does the effective strain transfer length for a given configuration. This trend is true for all bond layer thicknesses and epoxy moduli. A second conclusion relates to the effect of epoxy elastic modulus on strain transfer. It was observed that strain transfer increases with an increase in the adhesive elastic modulus. This trend supports the conclusions of previous studies, which suggest that the closer the elastic modulus is to the concrete, the better the strain transfer.

The results of this study suggest an inverse relationship between bond layer thickness and strain transfer. It is seen that smaller bond layer thicknesses provide greater strain transfer. Additionally, the effect of bond layer thickness appears to have more of an impact on the V-notch configuration than the saw-notch configuration. This behavior is likely due to the fact that the V-notch is wider with a tapered shape while the saw-notch geometry is narrower and more uniform. The bigger V-notch provides a greater volume of epoxy for strain loss to occur in. The tapered V-notch shape provides more epoxy between the FBG and the concrete than the saw-notch as the bond layer thickens.

FBG Sensors Mounted on Steel

Fiber Bragg gratings (FBGs) and traditional foil gages (TGs) were installed on an S3x5.7 steel beam. There were six of each type of sensor, where one FBG and one TG were located in six different locations on the beam. The averaged results from each FBG and TG set at the various locations were compared for the six tests. The modulus of elasticity values was used for comparison because the averaged results were linear, so one slope value accurately represented the data set.

Given the assumptions of the tests and additional test properties, the results are within a reasonable range. Typically, when comparing strain gages on the market to foil gages through laboratory testing, strain results within 5% are acceptable. Set 6 displayed this comparison with a 2% difference. However, based upon the assumptions and additional test properties, results within 15% are realistic.

1.3.2 Task 2

Upon study of the market for commercially available instrumentation, particularly FBG network interrogators, it became evident that a commercial product was superior to anything that could be developed individually. Commercial products provide the low-cost, compact form-factor and energy-efficiently required for this project. Additional pursuit of custom instrumentation would have been wasteful of research time and funding. Consequently, a two-channel SmartScan 02 Lite FBG interrogator developed by Smart Fibres was purchased for the laboratory study. This approach assured that the laboratory instrumentation conformed to the latest industry standards and had the reliability and durability

to perform as required. The only other resources required in the laboratory are a standard Windows-based desktop computer and an Internet connection.

Selection of instrumentation for field application was merged with task 3 in order to successfully integrate commercially available hardware with a custom-designed microcontroller. Findings and conclusions for the instrumentation intended for field application follow.

1.3.3 Task 3

Future field deployment and operation of the SHM network emphasized proof of concept of the radio frequency identification (RFID) triggering system for data collection and data storage capabilities. The research was focused on permitted vehicles. Additionally, the system was designed to correlate known vehicle data with the measured response of a bridge. The work focused on the RFID systematic description, the validation procedure, and the validation results for the proof of concept field tests.

The RFID system utilizes a transponder that wirelessly transmits data to and from the RFID tags. RFID transponders will be installed at a weigh station at a Wyoming port of entry and at the bridge of interest. At the port of entry, the permitted truck information, including the axle weights and configuration, will be assigned to an RFID tag with an identification code that would be placed on the windshield of the vehicle. Another transponder placed near the bridge will detect the presence of the RFID tag and trigger the system to store the bridge strain data when the tagged permitted vehicle passes over the bridge.

For the proof of concept testing, the triggering mechanism, data collection, and data storage were the specific parameters tested. The proof-of-concept tests were organized so that the initial positioning of each RFID component was established prior to testing the system at full speed, including positioning of the RFID transponder, RFID tag, and RFID vehicle. Each time the transponder detected the tag, the FBG strain data from three sensors were continuously recorded for the allotted 30-second time frame.

The proof-of-concept for the RFID triggering system was validated. It was determined that the success of the triggering is dependent upon the position of the tagged vehicle; the transponder, including the height and horizontal position; and the tag location in the vehicle. The proof-of-concept tests provided admissible results that were sufficient to move on to the next phase of instrumentation design and testing.

1.3.4 Task 4

The sensors installed on the concrete beam using methods developed in task 1 provided measurements similar to, but lower in magnitude than, what was predicted by the analytical model. It was necessary to account for averaging effects caused by the long gauge sensor configuration. Further discrepancies between the test results and the analytical model could be explained by a difference between the predicted and the as-built modulus of elasticity for the concrete.

The measurements taken on the steel beam were similar in magnitude to the values predicted by the analytical model. However, the measurements taken at different locations on the beam cross-section varied significantly, where they should have been similar. This variation could be explained by the presence of secondary load effects induced by an eccentricity in the load on the beam that was observed during the experiment. In a few locations on the steel beam, the sensors experienced a significant loss in pretension after installation. The wavelengths from these sensors did stabilize at a point that indicated there was still adequate pretension to make the necessary measurements. However, the resulting measurements at these locations appeared inconsistent with measurements taken from other sensors during the tests. This may be due to an inadequate bond between the sensor and the beam. However,

these sensors were located directly above the mid supports of the beam. So, the inconsistent measurements may have been the result of unpredicted localized effects from the supports.

1.3.5 Task 5

Based on the findings in the literature and additional testing with steel specimens in this research, it can be reasonably concluded that effective strain transfer in compression can be achieved with proper bonding technique. Whether the ineffective transfer with the wood block specimens was a consequence of micro-buckling or some other phenomenon remains unknown, and also irrelevant. The important finding is that FBG sensors can indeed perform accurately when subjected to compressive strain.

1.4 Recommendations

The research and development reported herein lays the groundwork for continued study involving field deployment of the FBG-based SHM system. The essential elements of the system are in place. These elements include the following:

- Sensor installation and protection techniques for both concrete and steel host structures
- Commercial and special-purpose instrumentation for interrogating the SHM network
- A novel triggering system based in RFID technology to control the amount of data that are collected from the SHM network.

Subsequent deployment of the system on a bridge in the WYDOT inventory will require additional development of data storage and transmission capabilities, which will be particular to the location and characteristics of the targeted bridge. In addition, the objectives of the SHM network (for instance, observing the impacts of overweight and other permit vehicles, validating load-rating software, monitoring long-term health of the bridge, etc.) will dictate the nature of the sensor installation, the type and volume of data collected, and the required post-processing requirements. Hence, development of a general performance specification for real-time data analysis is not feasible. Rather researchers engaged in Phase II of this study must coordinate with bridge engineers at WYDOT to identify a spectrum of SHM applications and objectives, for which individual data analysis techniques can be developed. Subsequent design and implementation of software to execute such data analysis will be needed to relieve bridge engineers from the burdensome and tedious tasks of sifting through raw SHM data streams themselves.

In addition to the general recommendation above to move toward field deployment of the SHM system, the following specific recommendations are offered.

1. Special attention should be taken when purchasing FBGs. Knowledge about existing technologies and manufacturers will help to assure accurate, consistent, and reliable strain sensor results. Particular points of interest include the wavelength range that can be sensed by the interrogator and the required spacing between central wavelengths of FBGs on an individual channel. The interrogator range and the spacing determine the number of sensors that can be installed on a single optical fiber.
2. In design of the sensor network for a particular bridge, sensors should be placed at a sufficient distance away from the neutral axis to ensure they are measuring meaningful flexural strain values. For many structures, the concrete deck will act integrally with the primary structural elements. This composite behavior (intended or otherwise) will shift the neutral axis toward the deck. Analysis should be performed for each structure to determine where the expected neutral axis will occur, and the neutral axis location should be considered when deciding where to locate the sensors on the cross-section.

3. A two-sensor configuration makes it difficult to distinguish any contribution from out-of-plane bending. If a sensor is located on a location of the cross-section where strains from one load effect act counter to strains from another load effect, these readings would underestimate the response of the structure to the loading. If these values were used to load rate a bridge, they would overestimate the capacity of the bridge. Placing the sensors close to the minor neutral axis of the beam would minimize the contributions from these secondary load effects. However, if there are significant secondary load effects, it would be important to consider them and the interaction of the stresses.
4. While the top flange of a girder is typically braced by the deck, the bottom flange often carries lateral loads along the girder line through bending until they reach a lateral brace that will transfer the loads into the deck. The significance of these lateral loads should be investigated as part of the design process for the sensor network.
5. The SHM system will be capable of recording massive amounts of data. It will be necessary to develop methods to automatically decipher which data are significant and should be transmitted and saved by the system. An algorithm to save data with readings that exceed a certain threshold or the maximum response each day may be appropriate. Taking a relaxed-state reading each day may be appropriate for documenting changes in the structure or to verify the functionality of the sensing system.
6. Since trucks pass over a bridge in a matter of seconds, it is highly unlikely that significant effects of temperature change will occur during the load event. Hence, when the data acquisition system is triggered by the RFID signal, initial relaxed-state scans of the bridge can be used to establish a baseline of strains immediately prior to and perhaps after passage of the permitted vehicle. Such an approach effectively embeds temperature compensation in the software that drives data collection rather than in special-purpose sensors, which require additional cost and bandwidth in the interrogator.
7. The RFID triggering system requires additional development. Developments include the port of entry system installation, firmware advancement, larger transponder range capabilities, cellular data transmission capabilities, database establishment, and software formation. For instance, use of the E-ZPASS system, common in many states, could simplify application of the system at the port of entry since it is already familiar to DOT officials and the trucking industry alike.
8. A database should be established that can manage a large amount of vehicle and bridge information and can be accessed by approved personnel, for example, WYDOT bridge engineers. Software as well as algorithms for automatic post-processing must be developed. One company that has been researched, Chandler Monitoring Systems, Inc., has developed some of these processes, and it may be worthwhile to pursue its guidance or services.
9. Port of entry sites would do well to couple weigh-in-motion systems to an RFID triggering system to automate collection of vehicle characteristics. Utilizing a static WIM system that already exists at the port of entries, bridge engineers can correlate that load to the bridge responses induced by permitted live loads.
10. Another possible enhancement to the SHM system could be a continuous load-rating system for permitted vehicles. Over time, a standard baseline could be built for specific permitted vehicles and bridge families. Instead of relying on a conservative analysis completed by Bridge Rating & Analysis of Structural Systems (BRASS) Girder, the actual responses would be measured and monitored for a variety of applied vehicle configurations. Algorithms and procedures would need to be developed to determine real-time bridge load ratings from bridge measurement data. By continuously monitoring the bridge, bridge management officials could potentially determine practices to safely increase the load ratings.
11. The SHM system could assist in identifying illegal loads and notifying law enforcement. Individuals or companies with overweight or oversize vehicles might not file for a permit in an attempt to bypass permit fees. Strain-level triggers implemented in the sensing network, coupled to RFID tags in trucks entering the state, could be used to detect and identify illegal loads.

2. PROBLEM DESCRIPTION

2.1 Problem Statement

State departments of transportation (DOTs) in the west have been under increasing pressure to permit and route overweight trucks transporting machinery and equipment for the energy sector through their state and interstate highway systems. DOT engineers are called upon daily to rate their bridges for overweight trucks to determine appropriate truck routing and to assess the impacts of the trucks on bridge safety and durability. Many of these overweight trucks have nonstandard configurations, which further complicates the rating and permitting process. Hence, it is critical that bridge engineers in DOTs develop confidence that their bridge analysis and rating software accurately predicts the response of bridges to overweight trucks, especially for bridges on the most frequently traveled routes.

The long-term objectives of this project were to develop and validate an instrumentation package for SHM of bridges subjected to overweight trucks and to develop plans for field deployment of the instrumentation on a pilot scale. Ultimately, the objective is to accurately correlate long-term field-performance data to the behavior of the bridges predicted by analysis and rating software. The field instrumentation package incorporates use of optical fiber sensors, specifically fiber Bragg gratings (FBGs), to monitor strains at critical locations in bridges that are considered most vulnerable to overweight truck loads and are most difficult to effectively rate with currently used software.

This report documents the methods and outcomes of Phase I of what is envisioned to be a long-term, multi-phase project. Phase I involved a laboratory investigation, the objectives of which were to develop the instrumentation package, remote data collection and processing capabilities, and field installation and operations methods suitable for long-term SHM of bridges in remote locations. Methods appropriate for both steel and concrete girder bridges were developed. The monitoring system is capable of observing bridge behavior under both static and dynamic (wheel impact) loadings.

Continuation of the research reported herein in Phase II of the project will extend the laboratory developments to field deployment and operations. It will further include correlation of field measurements with analysis results from bridge rating software. Key elements of Phase II will include configuration of the SHM system to properly record bridge response data for load events of interest, development of data transmission capabilities from the instrumented bridge to a central server (a process that will require site-specific details on bridge location, proximity to the central server, and availability of power and computer network access), and development of automated data post-processing methods to transform SHM data into formats that inform bridge engineers of the alignment of bridge performance with predicted results from their rating models.

2.2 Research Methods and Tasks

In Phase I of the project, instrumentation, packaging, installation techniques, and data collection and storage for fiber Bragg grating (FBG) sensors were to be developed in the laboratory. The laboratory investigation included the following primary tasks:

1. Development of optical-fiber packaging or other protection mechanisms suitable for installation in the target environments. Both steel and concrete girder bridges were considered, with emphasis placed on girder-line response. Considerations included the following sub-tasks.
    a. Protecting the optical fiber from damage due to the harsh environment and possible vandalism.

   b. Positioning and bonding optical fibers to the host girder material. The bonding process must assure effective strain transfer from the host material to the optical fiber in the vicinity of the FBG sensor.
   c. Repairing or replacing damaged optical fibers and sensors that do not survive the conditions in step 1.a.
   d. Compensating for temperature sensitivity of the FBG sensors, likely achieved through use of companion unbonded sensors.
2. Development of a low-cost, compact, and energy-efficient instrumentation package for interrogating the sensor network. The approach involved a combination of design and fabrication of custom instrumentation linked to commercially available components with proven reliability. This approach achieved a balance among cost, reliability, and ease of maintenance and replacement.
3. Development of data collection, processing, and transmission capabilities. An FBG sensor network on a bridge will have the capacity to collect an overwhelming volume of data, so much so that data storage and transmission could easily become a constraining bottleneck to the performance of the network. To avoid this bottleneck, real-time data processing is needed to convert the data collected by the interrogator into behavior parameters that are of value to bridge engineers at state DOTs. Among others such parameters may include strains, stresses, accelerations, vibration histories, damping ratios, and impact factors. The volume of even these behavior parameters could become overwhelming unless some control is provided to synchronize collection of the parameters with critical events, such as the passage of an overweight truck that has just been routed over the bridge, and then trigger delivery of the parameters to the DOT offices. For this project, a general performance specification for real-time data analysis developed in cooperation with bridge engineers at WYDOT was considered but regarded as infeasible. Design and implementation of software to satisfy site-specific performance requirements will complete this task in Phase II of the research.
4. Validation of tasks 1, 2, and 3 was performed in the laboratory using a mock-up of bridges having steel and concrete girders. Pseudo-static and dynamic loading protocols, intended to simulate slow-moving and high-speed truck traffic, were applied to the mock-up to excite the FBG sensor network. Observed response was then compared to detailed analysis results to confirm the function and efficacy of the SHM system.
5. Research outcomes during Year 1 of Phase 1, plus reports by other investigators, suggest that FBG sensors must be pretensioned prior to installation so that, if the host structure is subjected to in-service compressive strain, the sensors will simply relieve some amount of pretension, rather than experience a net compressive strain. Spurious compression-strain response of FBG sensors has been attributed to possible microbuckling of the optical fibers, thus rendering the sensor output unreliable as a measure of host-structure strain. This task involved an attempt to determine if microbuckling does indeed occur and what means can be employed such that microbuckling can be prevented, thus allowing the sensors to accurately respond to compressive strain.

2.3 Research Benefits

The proposed project will make direct positive contributions to the following strategic goals:

1. State of Good Repair: An effective SHM system for highway bridges will, over time, improve the ability of bridge engineers to predict the effect that overweight vehicles will have on the condition of their bridges. As engineers receive feedback on bridge performance to confirm or recalibrate their rating methods, they will have the capability to predict long-term durability of bridges. They will also be able to more effectively route overweight trucks and also specify appropriate reconfigurations of trucks that would otherwise not be permitted on certain routes.

2. Safety: Accurate real-time monitoring of bridge response will improve the operational safety of bridges during overload events by controlling the magnitude of the overload. Long-term safety will also be enhanced by use of the monitoring system to identify and quantify unanticipated overload events. Further, increased precision in defining the weight distribution in overweight trucks plus refinements in monitoring bridge response will reduce the inherent randomness in the demand (applied loads) as well as the variability in structural capacity to permit more refined predictions of bridge performance.
3. Economic Competitiveness: The proposed SHM system using relatively low-cost equipment with low power demand will provide the initial economic advantage to the project. The second advantage is in improved predictions of bridge durability and life-cycle. Effective scheduling of inspections and maintenance will be facilitated by an accurate and easy-to-use sensing network on the bridge. With suitable experience and calibration of the sensing network, engineers will be able to observe changes in bridge response that might suggest deterioration or damage, thus prompting more timely inspection and maintenance work. An SHM system that can be quickly deployed would be beneficial in instances in which a bridge may otherwise need to be restricted or closed due to advanced deterioration or impact damage. Monitoring a structure as the repairs are being designed could also help to ease the burden on the traveling public.

2.4 Literature Review

2.4.1 Background on Fiber Bragg Grating Sensors

Fiber Bragg Grating (FBG) strain sensors are beginning to achieve broad acceptance by the civil engineering field because they offer many advantages over other sensors available on the market (Zhou and Ou 2004). FBG sensors have been widely studied and used in structural testing and health monitoring applications, but are still less common than traditional foil strain gages because of the high cost of FBG sensors and interrogators. An FBG is an optical sensing device that consists of a grating etched into the core of an optical fiber at a precise spacing. When light is passed through the grating, a portion of the light is reflected back toward the source at a narrow band of wavelength centered about the Bragg peak wavelength. This process is illustrated in Figure 2.1. In the figure on the upper left, a broad spectrum of light enters the optical fiber from a laser or other light source. When the light spectrum encounters the FBG, a small portion of the spectrum, corresponding to the gage of the gratings, is reflected back to an interrogator. The rest of the spectrum passes through the grating as transmitted light.

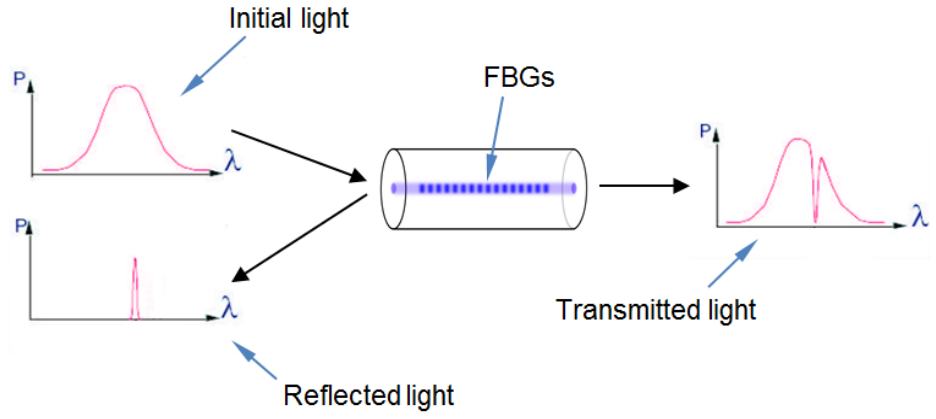

Figure 2.1 Illustration of FBG Signal Transmission (Heininger 2009)

A change in the pitch of the grating, which can be induced by straining the fiber, results in a shift in the peak wavelength that is reflected back. This shift in reflected wavelength is proportional to the str ain. Using this property, the strain in the fiber can be determined by measuring the shift in the reflected wavelength. The relationship between strain and wavelength shift is given by Equation 1.

$$\varepsilon = \frac{\lambda - \lambda_0}{G\lambda_0} \qquad \text{(Eq. 1)}$$

where: ε = strain
λ = reflected wavelength
λ_0 = unstrained reflected wavelength
G = gage factor (typically 0.78)

An interrogator is used to both send and receive the light signals for the gratings. The interrogator may have multiple channels, and multiple FBG sensors can be installed on a single fiber and interrogated by a single channel. Installing multiple sensors on one channel is called multiplexing. Multiplexing permits a large number of sensors to be installed on a structure and read by a single interrogator. Fibers can run the entire length of the structure and measure strains at multiple locations. Distributing a number of sensors along the length of just a few fibers simplifies the installation process and reduces the costs of equipment necessary to read the sensors. It is important to efficiently utilize the multi-channel and multiplexing capabilities of an interrogator in order to minimize the cost of an SHM system. Interrogators are by far the costliest components of an FBG monitoring system, accounting for as much as 70%of the component costs.

Because FBGs operate using light signals, the sensors are immune to electromagnetic interference, the behavior of the gage is extremely stable and does not need to be recalibrated (Guemes and Sierra-Perez 2013), and the signal can travel extremely long distances with almost no losses. Additionally, the silica material for the sensors is resistant to corrosion. So, the sensors can be applied almost anywhere as long as the optical fibers are protected from mechanical breakage.

Due to their many benefits and long lifespan, FBG sensors are beginning to be widely implemented in critical civil structures. Their benefits, however, may extend beyond just high profile projects and critical structures. As the technology becomes more widespread, the cost of FBG systems may reach a point where it becomes economically viable for widespread implementation of FBG-based bridge rating and monitoring systems on highway networks.

In summary, FBG sensors were selected for this application since they possess several advantages over alternative sensor technology. Some of these advantages include the following (Kreuzer, 2007):

- FBG sensors are effective in measuring strain to a high level of resolution. Changes in strain as small as 1 $\mu\varepsilon$ can be observed with suitable interrogation instruments and signal processing techniques. The sensors can further measure very high strains, in excess of 10,000 $\mu\varepsilon$, thus increasing the likelihood that they will continue to function in the event of severe damage, e.g., a vehicle collision with a bridge.
- FBG sensors are capable of high scan rates using relatively low-cost interrogation instruments. Frequency response rates of 5 kHz are easily achieved, allowing accurate determination of wheel impact factors.
- FBG sensors are immune to electromagnetic interference, which might otherwise limit the environments in which they can be used.
- FBG sensors can be interrogated over long distances (in excess of 5 km) without loss of signal strength and resolution.

- Multiple (25-50) FBG sensors can be located on a single optical fiber and interrogated with a single electronic device.
- FBG sensors, along with their interrogation instrumentation and data communications equipment, consume relatively low power, enabling an installation to function off-grid, using for instance a power supply consisting of only small solar cells and an automobile battery.

2.5 Transfer of Strain from Host Material to the FBG

A study by Pak (1992) had the objective to determine strain transfer behavior of a fiber optic sensor (FOS) strand embedded in an isotropic homogeneous host matrix with an applied longitudinal shear stress. A numerical analysis was conducted in which various material property relationships of the fiber and host matrix were compared. Pak considered two types of embedded fibers: one with a single layer coating and a second bare embedded fiber with no coating. Different thicknesses and shear moduli of the coating and fiber were tested in order to observe strain transfer variations. The results led to several relevant conclusions contributing to the understanding of the elastic behavior between an embedded FOS and its host material.

The most relevant trends seen in the study were derived from a comparison of the shear strain transfer in the optical fiber with various shear moduli and thicknesses of the fiber coating. It was found that strain transfer increased in the optical fiber as the coating layer got thinner but only when the shear modulus of the coating was less than that of the host matrix. Conversely, when the shear modulus of the coating was greater than that of the host matrix, the shear transfer increased as the coating layer got thicker. This relationship allowed determination of the shear modulus of the coating, which gives the greatest shear transfer to the fiber. The maximum shear transfer from the host material to the fiber occurs when the shear modulus of the coating is the geometric mean of the shear moduli of the host matrix material and the fiber. This relationship is true for all coating layer thicknesses.

Further analysis of the results showed that the most accurate shear transfer would occur if the bare fiber were embedded directly into the host matrix without a protective coating. As stated previously, the shear transfer across the coating improves as the coating gets stiffer; however, since in most applications the coating (typically epoxy or plastic cladding) is less stiff than the host material (typically steel or concrete), it is correct to assume that the optimal fiber embedment configuration would have no coating. Furthermore, for a fiber with no coating, it was found that the best shear transfer occurs when the optical fiber stiffness is equal to or less than that of the host matrix material. The study conducted by Pak discovered several fundamental relationships about embedded fiber optic sensors that are useful in their implementation and optimization in civil engineering applications.

Zhou et al. (2010) investigated axial strain distributions of FBG sensors and the influencing parameters, which include the bonded length of the FBG sensor, adhesive thickness, and elastic modulus of the adhesive. Zhou et al. considered a four-layer cylindrical model consisting of the inner core of bare optical fiber sequentially wrapped by a protective coating, an adhesive layer, and an outer host material.

A finite element analysis was conducted to examine the strain transfer from the outer host material to the FBG core under an axial tensile stress of 50 MPa applied to the host material. The results of the FEA were then verified by laboratory testing of the FBG strand bonded to an aluminum alloy dog-bone specimen. The mechanisms that induce FBG chirping phenomena were also identified and analyzed. Chirping is a phenomenon that occurs when the period of the gratings along the grated section of the fiber is not constant. Chirping results in inaccurate sensing because the reflected wavelength was formed by inconsistent grating periods.

The laboratory tests conducted by Zhou not only verified the FEA results but also revealed some insightful information about the chirping phenomena. Three dog-bone specimens were tested with adhesive bond lengths of 5 mm, 10 mm, and 15 mm. The effective sensor lengths found for each specimen corresponded well with those found in the FEA. It was found that increased chirping occurred as the bond length decreased. When the bond length was equal to the grating length (5 mm), the chirping was unacceptably high; but when the bonded length was three times the grating length (15 mm), chirping was nearly nonexistent. Therefore, it was concluded that a bonded length that is at least three times the grating length will minimize chirping and provide optimal strain transfer sensing.

Zhou's study discovered several important characteristics dealing with strain transfer of embedded FBG sensor. FBGs can be designed for optimal strain transfer as long as the material properties, bond configurations, and grating lengths are all properly set. Additionally, it is best to have a stiff adhesive layer that is as thin as possible but still provides an adequate bond.

The ability to determine the amount of strain transfer from a host material to the fiber core of a fiber optic sensor (FOS) is the subject of interest in a study by Ansari et al. (1998). In their research, a theoretical model was developed that calculates the strain in a host material using the values measured by an FOS. The investigation considers the strain loss through the protective coating of an FOS as well as the behaviors of a bare embedded FOS. The theoretical model is verified through experimental tests of FOS strands attached to a tapered cantilever beam. Results of the study suggest that strain transfer is a function of the mechanical properties of the fiber core, the protective coating, and the fiber gage length (length of optical fiber in contact with the host material). The result of this research makes it possible to determine FOS gage length requirements, but also eliminates the need for calibration tests and statistical analysis to determine strain transfer. It was also found that having a bare embedded fiber (no protective coating) gives an optimal strain transfer, but is an unrealistic configuration due to the requirement for fiber protection when used in structural health monitoring applications.

The goal of the analysis conducted by Torres et al. (2010) was to understand the effectiveness of a new FBG packaging system that was adhered to the surface of a host structure. The packaging configuration consists of an FBG fiber covered by a single protective layer of composite material made up of glass fiber reinforced polyester resin. A second more common configuration was also tested and used as a comparison to the new configuration. The second configuration had two protective layers of the glass fiber composite material, one on each side of the fiber. The two configurations were adhered to a host structure using a thin layer of adhesive. A finite element model (FEM) of the packaging was used to determine the configuration that produces optimal strain transfer between the host structure and the FBG sensor. The parameters that were adjusted in order to optimize the design included material properties, adhesive layer thickness, temperature, and the number of protective layers. A strain was applied on the lower face of the adhesive layer, which simulated strain induced in the host structure caused by temperature change. The response of the system to the induced strain was analyzed assuming an orthotropic adhesive layer, and only considering thermal expansion in the longitudinal direction.

A comparison of the new single layer packaging design and the more commonly used double layer design resulted in strong partiality towards the single layer configuration. The presence of a second 400-μm-thick protective composite layer between the fiber and the host structure caused a substantial strain transfer error of 15%. In addition, the extra layer caused an inconsistency in strain transfer measurements, which was thought to be a result of material manufacturing defects and material property variances. The single layer design not only eradicates this error but is also a simpler design.

2.6 FBG Sensor Placement

For the purpose of performing load tests on bridges, the Manual for Bridge Rating through Load Testing (A.G. Lichtenstein and Associates, Inc. 1998), published by the National Cooperative Highway Research Program (NCHRP), states that sensors should be placed on critical members and in locations to gather data that can be used to verify the analytical model. In the following, a three-digit notation of the form X.XX is used to describe a point of interest (POI) on a bridge. The number on the left of the decimal place indicates which span the POI is located in, and the two-digit number to the right of the decimal place indicates how many tenths of the span the POI is from the left end of the span. For example, 1.00 indicates a position just inside of the first support of a bridge. Location 1.05 describes the middle (5/10) of span 1, and 1.10 describes the location just to the left of the second support. Location 2.00 would then describe the location just to the right of the second support.

In Barker et al. (1999), six different standardized testing plans are detailed for measuring the different factors that can affect a load rating on a steel girder bridge. These testing plans provide guidance for placing the necessary sensors for performing the required tests. The six plans vary in complexity and effort required based on the amount of information the tester would like to gain from the test. The simplest plan consists of a single strain gage placed on the bottom flange of the critical girder at the location of maximum moment determined from analysis. This simple plan can be used to post a bridge. The most complex plan consists of multiple sensors on each of the girder webs at the maximum moment regions and near each support. This more complex configuration can be used to determine load rating adjustments for: impact, lateral load distribution factors, bearing restraints, and composite behavior.

Chajes, Shenton III, & O'Shea (2000) performed diagnostic load tests on a bridge by placing sensors on the top and bottom flanges of girders at the middle of each of the three spans in a continuous multi-girder bridge. They did not discuss any analysis indicating that the mid-span locations were points of maximum load effect, and typical practice would indicate that the sensors in the exterior spans are not measuring the maximum load effects. The AASHTO Bridge Design Manual (AASHTO 2012) reports statistical moment data from the 1.04, 2.05, and 3.06 span locations from a number of bridges in the commentary discussing the calibration of the HL-93 live load and load factors. These span locations reflect a commonly accepted rule of thumb for estimating the anticipated maximum moment locations in a three-span bridge.

In Cardini and DeWolf (2008), sensors were placed on the web of the steel girders. They were located 2 inches below the top flange and 2 inches above the bottom flange. This placement allowed for the calculation of the neutral axis location. However, by being further from the extreme fibers, the strain gages were limited to measuring smaller strains. As it was a simple-span bridge being tested, sensors were installed only at mid-span for each of the girders on the bridge.

Doornink, et al. (2006) conducted a study to monitor a bridge for local failure in a girder web by placing sensors across the region of the expected failure and in other “non-target” areas. By tracking the paired response of these sensors to loading events over time, they were able to prevent false alarms that could have been triggered by systems monitoring sensors in the critical locations alone.

In addition to placing sensors to measure critical member behavior, Seo, Phares, Lu, Wipf, & Dahlberg (2012) placed sensors on the underside of the bridge deck in order to determine the approximate wheel locations and axle spacing of a vehicle during a load event.

2.7 FBG Sensor Installation

Several considerations are important when determining an appropriate sensing system for bridge monitoring and testing. A good summary of issues to consider is presented in Farhey (2005). Many of the complications described in this summary are overcome by FBG sensors. However, the developed system must still consider appropriate sensor placement, ease of installation, gauge lengths, and procedures for protecting and replacing sensors. In addition, FBG sensors present some additional challenges that are not discussed by Farhey, such as appropriately tensioning fibers and adequately spacing the wavelengths of multiplexed sensors. These challenges are addressed below.

The FBG sensors used in the study by Todd et al. (1999) were installed on steel girders using a cyanoacrylate adhesive and protected with a silicone RTV sealant. This method of protection is simple to apply and provides protection from weather. However, it may not be adequate to withstand vandals and wildlife.

In Doornink et al. (2006), FBG sensors were embedded in carbon fiber reinforced polymer packaging, which is commercially available, and installed on steel bridge members using cyanoacrylate adhesive. The strain measurements showed excellent agreement with the traditional strain transducers that were installed to verify the accuracy of the FBGs.

A different type of fiber optic sensor, called a Brillouin Optical Time-Domain Reflectometry sensor, was used in Matta et al. (2005). The installation required for this type of sensor is similar to that required for FBG sensors. For this study, the researchers ordered the fibers to be factory-embedded into an FRP tape. The sensors and tape were then adhered to the steel bridge girders using a two-part epoxy encapsulation resin. Prior to adhering the sensors, the steel was prepped by manually roughening the surface with steel brushes and applying a lacquer thinner for degreasing.

2.8 FBG Protection Techniques

A presentation by Micron Optics, one of the leading FOS manufacturers in the United States, describes general misconceptions about the reliability of FOS (Micron Optics, 2014f).

1. A sense that FOS is still a “research” technology.
2. Prior direct or anecdotal poor experiences with university or startup technology and/or deployments.
3. Prior poor experiences stemming from inadequate understanding or training with regard to FOS strengths, weaknesses, and deployment techniques.

Various topics have been explored by Micron Optics, including fiber breakage susceptibility, poor or inconsistent strain transfer from carrier to FBG, spectral distortions leading to measurement distortions, fiber or carrier creep, fiber debonding, repeatable thermal response, humidity exposure and cycling, and fatigue cycling. Micron Optics laboratory and field qualification tests have proven that the right materials, processes, and controls can provide accurate and reliable strain results (Micron Optics, 2014f).

The protective coating on an FBG must be removed in order to etch the grating into the core of the fiber, which designates a base wavelength for that specific fiber. Afterward, the FBGs must have their inner cores protected by recoating the fiber, enhancing the fiber’s strength and flexibility. The two most common types of recoating material currently available are polyimide and acrylate. Kuang, et al. (2006) at the National University of Singapore studied the performance of FBGs embedded in carbon fiber composites; some were recoated with acrylate and some were bare FBGs after the recoated acrylate was removed. It was discovered that the bare FBGs performed more accurately compared with the recoated

acrylate fibers, which saw a significant amount of stress relaxation. A study completed by the University of Manitoba (Rivera et al. 2005) discusses the main differences between polyimide and acrylate recoating. Tension tests were conducted for strain transfer performance; the FBGs were purchased from two different manufacturers, and the results were dependent on the manufacturer, not the type of recoat material. This finding led the researchers to believe that FBG recoating standards should be implemented. An e-mail from a representative at Micron Optics (Baez, 2014), one of the leading FBG manufacturers in the United States, described acrylate recoat as a "spongy" cladding, commenting that polyimide coating accomplishes strain transfer more successfully and has a wider temperature range.

2.9 FBG Strain Verification Cases Based upon Laboratory and Field Testing

Fiber optic sensors were first applied in the 1960s for commercial telecommunication purposes. They have been utilized in military and aerospace equipment fields, and have, within the last two decades, begun to gain acceptance into many fields including health monitoring for medicine and various engineering fields. In the civil engineering industry, they are ultimately used to potentially increase the life of expensive and important structures as well as avoid crucial failures (Annamdas, 2011).

Ansari (2007) discussed the complications in using bare FBG sensors, or sensors without a type of carrier or protection method in field conditions. In Hong Kong, China, 40 sensors were installed on the Tsing Ma Bridge to measure temperature and strain. By using epoxy and a nitinol metal as a protection method, favorable strain results were seen from testing, agreeing with traditional foil gage measurements in similar locations (Chan et al., 2005). Tests completed by a team at the University of Iowa Bridge Engineering Center displayed good agreement between FOS and traditional foil gage strain readings, which assured accuracy for field instrumentation on the U.S. 30 Bridge near Ames, Iowa (Doornink, 2006). This study showed that FBGs perform accurately using a variety of different protection techniques.

Bridge Diagnostics Inc. (BDI) of Boulder, Colorado, was hired to install its strain sensors adjacent to the FOS installed on the U.S. 30 Bridge to compare readings based upon ambient traffic loads. The results from BDI's sensors and the FOS were excellent, and the tests were deemed successful (Doornink, 2006). During construction of the Hulanhe Bridge, which crosses the Hulan River in northeast China, 15 FBGs and 15 traditional foil gages were installed. The FBGs performed as expected while only one traditional foil gage survived the installation procedure, proving the durability and reliability of FBGs over foil gages in this application (Zhou et al.).

ISIS Canada and the University of Manitoba teamed up to install FOS onto various bridges in Canada (Tennyson, 2001). The Beddington Trail Bridge in Alberta, Canada, was an example of FBGs as a reliable strain sensor with 18 out of 20 sensors still working accurately three years after installation. The Taylor Bridge in Manitoba, Canada, was used to install 63 FBGs with traditional foil gages used to compare the data. Only 40% of the foil gages survived while the majority of the FBGs were still reading accurately.

3. OPTICAL FIBER PACKAGING

Task 1 for this research project involved development of optical-fiber packaging or other protection mechanisms suitable for installation in the target environments. Both steel and concrete girder bridges were considered, with emphasis placed on girder-line response.

3.1 Bonding to a Concrete Host

The elasto-mechanical problem involving use of FBG sensors in concrete host structures was studied by Maurais (2012). That study involved both experimental testing and FEM analyses to determine the strain transfer behavior of FBG sensors embedded in notches in the concrete host. Other researchers have examined strain transfer behavior of FBG sensors embedded in concrete as it is cast. By contrast, this research focused on installation of the sensors in existing structures, rather than during the construction sequence.

3.2 Finite Element Study

A three-dimensional finite element analysis (FEA) of a notched concrete host structure and a notch-embedded FBG strand (Figure 3.1) was conducted to study strain transfer behavior from the concrete to the FBG. The 90-degree V-notch configuration in Figure 3.1 shows an optical fiber with FBG sensors embedded in an epoxy-filled V-shaped notch. The V-notch configuration was studied, as the V-notch may be formed when the concrete host structure is cast or may be cut in after the concrete has cured, providing the opportunity for optical fiber installation following construction. The saw-notch configuration in Figure 3.1 involves a bull-nosed slot cut into the concrete after construction using a conventional abrasive saw blade. Again the optical fiber with its FBG sensors is bonded within the epoxy-filled notch. Bond layer thickness, adhesive bond length, adhesive elastic modulus, and notch geometry were all variables of interest in the study.

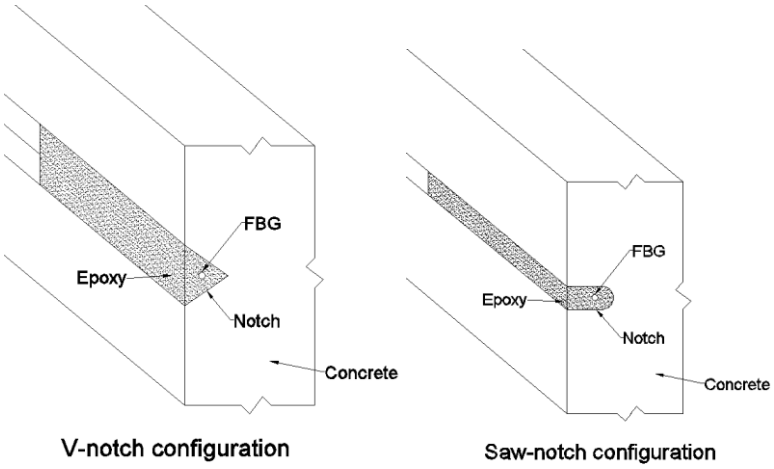

Figure 3.1 Notch embedded FBG configuration cross sections

Each notch configuration was modeled with a different FEA model. Figure 3.2 illustrates the two models, which exploit the quarter-symmetry of the notch configurations. The red line in the figure represents the optical fiber, which lies in the plane of symmetry. The light-gray elements represent the epoxy and the dark gray elements represent concrete.

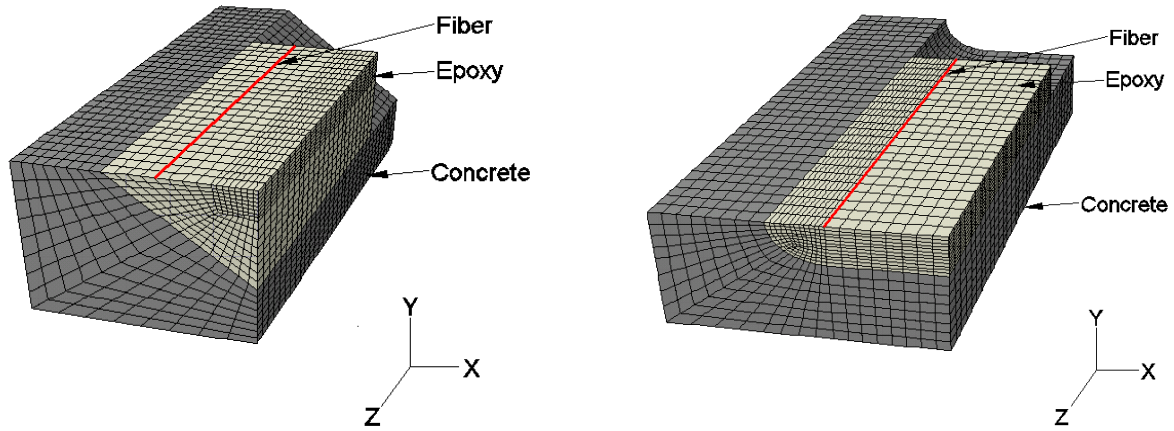

Figure 3.2 (a) V-notch FEM configuration, (b) Saw-notch FEM configuration

The epoxy bond length and bond layer thickness are two important parameters that affect strain transfer. The epoxy bond length is the length of epoxy in the concrete notch measured parallel to the optical fiber and bonds it to the concrete. Intuition suggests that the longer the epoxy bond length the better the strain transfer; however, it is theorized that only a portion of the optical fiber needs to be bonded in the notch in order to achieve full strain transfer. Epoxy bond lengths of 10 mm, 20 mm, 30 mm, 40 mm, 50 mm, and 60 mm (0.4 in, 0.8 in, 1.2 in, 1.6 in, 2.0 in, and 2.4 in) were analyzed in the FEA in order to determine which lengths provide full strain transfer to the FBG. The bond layer thickness is the distance from the epoxy embedded fiber to the tip of the concrete notch. It is hypothesized that as bond layer thickness increases, i.e., the fiber moves further away from the notch tip, the strain transfer from the concrete to the fiber will decrease. To test this hypothesis, the strain transfer was analyzed with thicknesses of 0.875 mm, 1.75 mm, and 3.5 mm (0.034 in, 0.069 in, and 0.137 in) for the V-notch configuration and 1.6 mm and 3.2 mm (0.063 in and 0.126 in) for the saw-notch configuration. All the bond layer thicknesses were tested for each epoxy bond length, giving 18 different configurations for the V-notch and 12 configurations for the saw-notch.

The elastic modulus of the epoxy also has an effect on strain transfer. Studies discussed in the literature suggest that the closer the elastic modulus of the epoxy is to that of the host material (concrete), the better the strain transfer will be. Four different epoxy moduli were used in each of the aforementioned configurations to determine the relationship between epoxy modulus and strain transfer. After researching various epoxies that would be suitable for field applications, the following four elastic moduli were selected: 700 MPa, 1800 MPa, 3000 MPa, and 6000 MPa. Each elastic modulus was tested for all the FEM configurations, giving a total of 72 configurations for the V-notch and 48 configurations for the saw-notch. The elastic moduli for the concrete and FBG were modeled as 25,000 MPa and 72,000 MPa, respectively. Strain was induced in the concrete part of the FEM by applying an axial displacement to the free end of the concrete. Boundary conditions were applied to enforce symmetry. A perfect bond was assumed to exist between the concrete and the epoxy and between the epoxy and the fiber.

Strain transfer from the concrete over the epoxy bond layer to the fiber is the primary behavior parameter of interest. The strain transfer ratio r is represented as the ratio of the strain in the fiber to the strain in the concrete at adjacent locations in the model. In addition, the strain transfer values at all nodes along the length of the fiber were determined to identify the *effective strain transfer length* l_e for a given model configuration. The effective strain transfer length is the length along the fiber that is experiencing fully developed strain transfer i.e., $r = 1.0$. In order to determine l_e of each configuration, the strain transfer along the length of the fiber was calculated and plotted.

As a sample of the FEA results, Figure 3.3 illustrates the relationship between strain transfer ratio and the distance from the center of the FBG sensor in the saw-notch FEA model with a 1.6 mm (0.063 in) bond layer thickness and the epoxy bond lengths listed above. Each of the haystack-shaped curves in the figure is for a different epoxy bond length. As shown in the figure, an increase in epoxy bond length results in an increase in strain transfer ratio up to a value near 1.0. The haystack curves also flatten out with increasing epoxy bond length to illustrate the length over which full strain transfer occurs. The effective bond length is then defined as the length of the flat portion of the haystack curve. For a given model configuration to be fully effective in terms of strain transfer, the flat portion of the strain curve must be at least 10 mm long, which is the length of the grated sensor region in the FBG. Additional illustrations of the FEA results are found in the report by Maurais (2012).

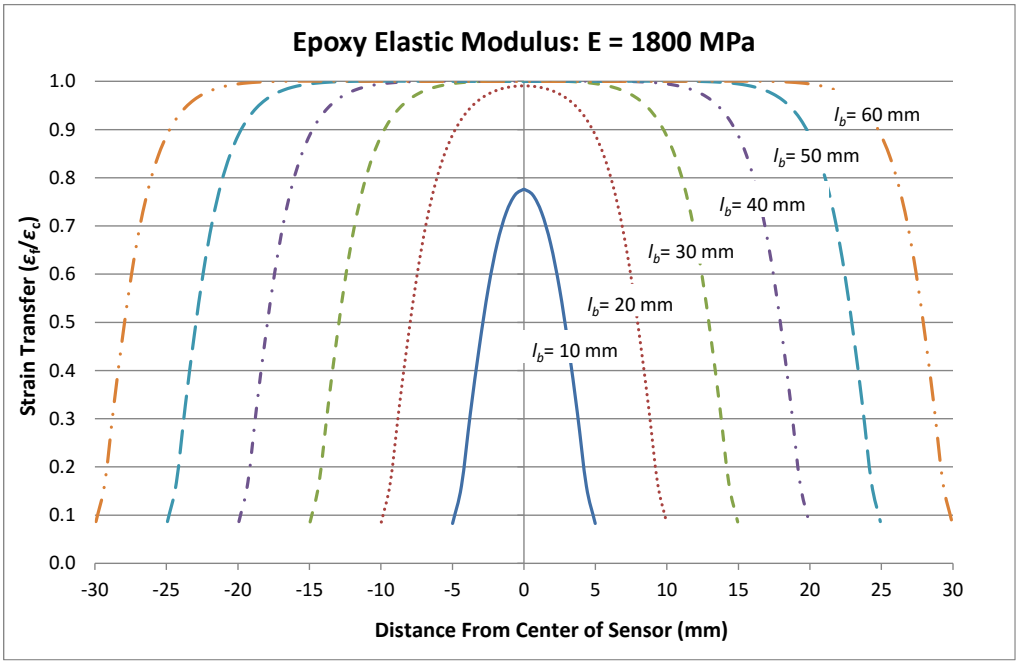

Figure 3.3 Epoxy bond length comparison, saw-notch, 1.6 mm bond layer thickness

It is interesting to note that the amount by which the strain transfer decreases as bond layer thickens is greater for the V-notch than the saw-notch. This behavior is likely because the V-notch is wider with a tapered shape while the saw-notch geometry is narrower and more uniform. The bigger V-notch provides a greater volume of epoxy for strain loss to occur in. The tapered V-notch shape causes the strain transfer to reduce more than the saw-notch as the bond layer thickens.

3.3 Experimental Study

An experimental study was conducted on notched concrete prisms with adhered FBGs and conventional strain gages. The objectives of the tests were to confirm the results from the FEA as well as to develop an FBG application technique suitable for field implementation. Two types of concrete prisms were cast, both having the same dimensions but with different notch geometries. One prism type had V-notches and the other had saw-cut notches, with notch geometries matching those of the FEM. The prism dimensions were 20 cm x 10 cm x 10 cm (8 in x 4 in x 4 in) with one longitudinal notch on each of the four sides as seen in Figure 3.4. The prisms were notched on all four sides so that multiple fibers could be imbedded and tested simultaneously on the same prism.

Figure 3.4 Concrete test prisms notches: (a) V-notch (b) Saw-notch

The FBG strain sensors were embedded into the notches of the concrete prisms in order to observe the strain transfer behavior from the loaded concrete prism to the FBGs. The prisms were axially compressed using an Instron 1332 servohydraulic loading machine. The FBGs were embedded into the prism notches using a common structural epoxy with an elastic modulus of 1800 MPa (Ultrabond 1300 manufactured by Adhesives Technology). Data from surface-adhered conventional strain gages were used to compare with the epoxy-embedded FBG strain data to establish strain transfer rates. The strain measured by the conventional strain gages was taken as the strain of the concrete in the comparison. Additional details of the test set-up and loading protocols are found in Maurais (2012).

Figure 3.5 is representative of the results of the experimental study compared to the FEA results. In the figure, the haystack curve from the FEA V-notch model with 30 mm (1.2 in) epoxy bond length, 2.7 mm (0.106 in) epoxy bond layer thickness, and epoxy modulus of 1800 MPa (261 ksi) is compared to the strain transfer ratio from the companion experimental test. In the figure, the short dashed line represents the experimental strain transfer ratio. The dashed line is a 10 mm (0.39 in) line segment, because the strain transfer of each experimental test was taken as a single averaged strain value. The 10 mm (0.39 in) segment represents the strain transfer to the 10 mm (0.39 in) FBG sensor region that was centered in the epoxy.

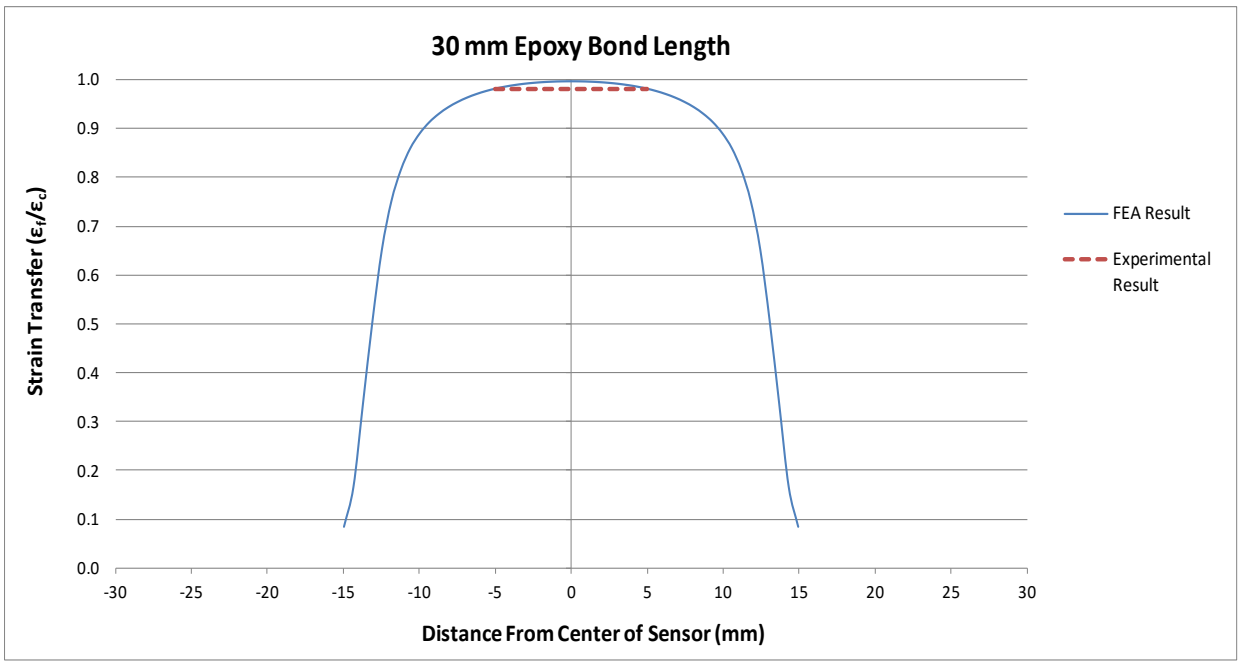

Figure 3.5 Strain transfer for V-notch, E_{epoxy} = 1800 MPa, 2.7 mm bond layer thickness

As shown in Figure 3.5 and in general, the FEA models predict slightly higher strain transfer ratios than the experimental test. A few influencing factors include the assumption of perfect bond in the FEA models, the influence of aggregate size in the concrete creating a nonhomogeneous strain state at the FBG sensor, the use of form oil on the concrete surface that might soften the bond between the epoxy and the concrete. Nevertheless, the experimental results match well with those from the FEA models, confirming that FEA modeling can be used reliably to predict the strain transfer behavior of notch-embedded FBG sensors in concrete.

3.4 Bonding to a Steel Host

Verification of the strain transfer behavior of FBG sensors when adhered to a steel host was performed experimentally on a small four-point bending specimen (S3x5.7 cross section). The basis of comparison of FBG performance was that of traditional foil strain gages (TGs).

Micron Optics os3120 FBG sensors were selected for application with the steel host material. These sensors were chosen because they are protected by a steel carrier, installed easily with an epoxy, and used frequently in the field. This approach is beneficial as opposed to a spot welding model, because field welding on WYDOT bridges is prohibited. Micron Optics provides the following performance properties for the os3120 gages (Micron Optics, 2010a):

- Strain sensitivity ~1.4 pm/με
- Gage length = 22 mm 0.866 in)
- Operating temperature range = -104° to 248° C (-155° to 478° F)
- Strain limits +/- 2,500 με
- Fatigue life = 100(10^6) cycles, +/- 2,000 με

Both FBG and TG sensors were adhered to the steel specimen using Micron Optics' recommended procedures. Sensors were placed at the following locations on the S3x5.7 beam specimen:

- Set 1: On the top surface of the top (compression) flange at mid-span over the web
- Set 2: On the bottom surface of the top flange at mid-span near the tips of the flanges
- Sets 3 & 4: At mid-depth of the cross section between load points and support points, oriented at 45 degrees from horizontal to measure shear strain
- Set 5: On the top surface of the bottom (tension) flange at mid-span near the tips of the flanges
- Set 6: On the bottom surface of the bottom flange at mid-span over the web

Additional details of the test specimen, set-up, and loading protocol are found in the thesis report by Danforth (2015).

Test results are mixed, in that, at a given load on the beam, in some cases the FBG sensors recorded higher strains than the TG sensors and other cases the FBG sensors recorded lower strains. As a representative illustration of the test results, Figure 3.6 contains the stress-strain curves for the FBG and TG sensors in set 1 – on the top surface of the top flange (loaded in compression). At a given applied stress, the FBG sensors record higher strains than the TG sensors. Nevertheless, the two curves track fairly uniformly and nearly linearly. Accuracy in placement of the sensors on the relatively small test specimen is the likely reason for the differences in behavior. However, in all cases, the results from the FBG sensors are reasonable and provide confidence that they will perform adequately in a field application.

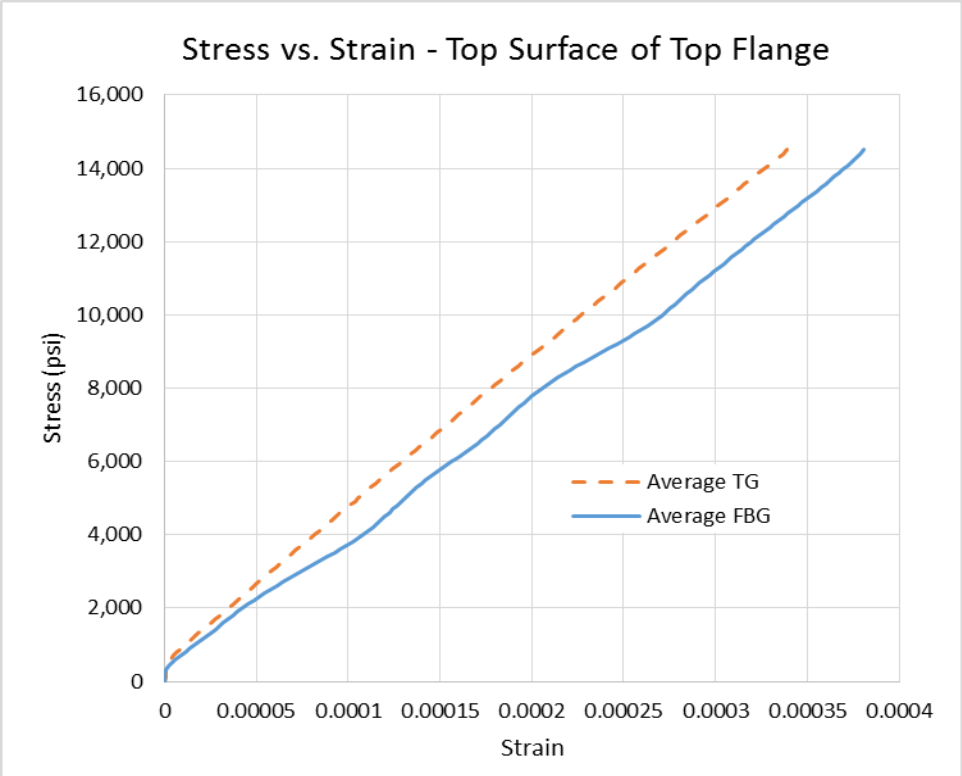

Figure 3.6 Stress-Strain Comparison, Steel Specimen

4. INSTRUMENTATION PACKAGE

Task 2 involved development of a low-cost, compact, and energy-efficient instrumentation package for interrogating the sensor network. The approach involved a combination of design and fabrication of custom instrumentation linked to commercially available components with proven reliability. This approach achieved a balance among cost, reliability, and ease of maintenance and replacement.

A commercially available interrogation system was selected for proof of concept laboratory testing. A two-channel SmartScan 02 Lite FBG interrogator developed by Smart Fibres was purchased to interrogate the sensor network in the laboratory. The only other resources required in the laboratory are a standard Windows-based desktop computer and an Internet connection.

For field application, we selected the four-channel FS2200XT BraggMETER from FiberSensing. The FS2200 extended temperature interrogator features high bandwidth, programming capabilities, Ethernet interface, and ability to handle harsh Wyoming weather. A custom microcontroller system to operate the BraggMETER interrogator was developed and implemented specifically for unattended, remote deployment at a bridge site. Details of this system are presented in the following chapter.

5. DATA COLLECTION AND PROCESSING

Task 3 involved development of data collection, processing, and transmission capabilities. An FBG sensor network on a bridge will have the capacity to collect an overwhelming volume of data, so much so that data storage and transmission could easily become a constraining bottleneck to the performance of the network. Compounding this problem, the need to sift through the huge amounts of data to locate and use behavior parameters of interest would be an overwhelming and tedious task for bridge engineers.

The first step in dealing with this challenge is to develop an interrogation control system that activates the SHM network interrogator only when needed and successfully stores the network data. Unattended operation of the system is essential to eliminate the need for DOT personnel to be at the bridge site with permit vehicles or if other extreme events occur. A microcontroller system was developed as part of this research that satisfied the preceding first-step requirement.

Since Phase I of the research did not include deployment of the SHM network on a prototype bridge, it was not feasible to pursue further development of a real-time data processing and transmission capability. Such development will be specific to the particular bridge location, access to data networks, electrical power, and the performance parameters that are critical for the bridge. Hence continuation of this task must become a component of Phase II of the envisioned future research. That is to say, it was not possible to develop a general performance specification for real-time data analysis of an arbitrary bridge. Instead, site-specific specifications must be developed in cooperation with bridge engineers at WYDOT. Subsequent design and implementation of software to satisfy the performance requirements will complete this task.

For Phase I of this research, an Ethernet-to-SPI (Serial Peripheral Interface) data link was established to the microcontroller from the interrogator through two Olimex mod-enc624J600 boards, which are composed of Microchip's ENC624J600 10/100 Base-T Ethernet controller. The established SPI connection allows access and discrimination of streaming raw data through the use of an Atmel ATXMEGA64A3 microcontroller. The microcontroller was programmed with firmware triggers based on predetermined parameters in order to alleviate data bottlenecks and over-storage that inevitably occur as a result of transmission speed differences between the interrogator and the Ethernet transmission device, as well as storage limitations associated with the unsegregated collection of data. Local post-filtered data storage was accomplished by an SD-card board also supplied by Olimex.

When the system is deployed for field application, it will have the capacity to implement remote data storage by software on a dedicated computer or server as data are received through the Ethernet module. Two examples of Ethernet modules considered include radios or cellular gateways. Two cellular Internet gateway modules have been considered: the OnCell G3150 by MOXA and the Airlink Raven XT by Sierra Wireless, which was recommended by Mr. Keith Tupper with WYDOT. Both systems are suitable for industrial Supervisory Control and Data Acquisition (SCADA) applications. The selection of the gateway will be determined when the system is deployed in the follow-up project. The connection from the microcontroller to the cellular module will be accomplished through an SPI connection using another Ethernet controller, which converts the SPI signals back to the Ethernet for transmission.

Also of major importance is selection of a suitable power source from which the previously mentioned instrumentation will draw. Two primary methods have been considered. One option, assuming the equipment will be located close to a power grid source, is to connect directly to the grid. The second method under consideration would be the implementation of a solar panel with a bank of batteries.

Finally, a novel triggering mechanism has been developed to initiate data collection from the sensor interrogator and network. We have selected a radio frequency identification (RFID) tag reading system that employs passive RFID tags in the overweight vehicle to activate the data acquisition system. This approach will facilitate live, unscheduled collection of data for all permitted vehicles. The RFID tag can be placed in the cab of the permitted vehicle at the port of entry. Then the SHM system will automatically detect and record passing of the vehicle over the bridge. Bridge response data will be collected and transmitted as required to facilitate analysis of bridge response to the passing vehicle. The RFID system, supplied by Convergence Systems Limited, has been integrated with the microcontroller to activate data recording from the interrogator. For the system to function as intended, the interrogator must remain continuously active.

5.1 Microcontroller and RFID Triggering System

One challenge with managing a continuous, long-term bridge monitoring system is collecting, storing, and prioritizing the copious amounts of bridge response data. The RFID triggering system was developed as a method to prioritize the collection and storage of data by triggering the system with a predetermined and recognizable vehicle. The triggering is important because storing continuous strain data can result in an unmanageable amount of information to be stored or to be passed through a cellular modem. The outcome of the system would provide the means to collect and store only the meaningful FBG strain data.

5.1.1 System Overview

The RFID system operates by transferring information using radio-frequency electromagnetic fields, utilizing a transponder that wirelessly transmits data to and from the tags. In this specific application, RFID reader and antenna combinations, or transponders, will be installed at a weigh station at a Wyoming port of entry and at the bridge of interest. At the port of entry, the permitted truck information, including the axle weights and configuration, will be assigned to an RFID tag with an identification code. The tag would then be placed on the windshield of the vehicle. At the bridge, a different transponder will detect the presence of the RFID tag and will trigger the data acquisition system to store the bridge strain data while the permitted vehicle passes over the bridge. The following subsections describe the process in detail.

The first transponder should be placed at a Wyoming port of entry. Along with detecting the presence of a tag, the transponder has the capabilities of writing specific information to a tag, enabling a transponder to read the data from the tag at a different point in time. All permitted vehicles are required to stop at the ports of entry when crossing over the state line to assure that they remain in compliance with their specified axle loads and gross vehicle weight requirements. When a permitted vehicle is weighed, it will be assigned a tag encoded with a vehicle identification number. At the weigh station, the axle weights, gross vehicle weight, and axle configuration will be determined. This information can then be entered into a database and associated with its assigned vehicle identification number. The vehicle will then travel across the highway with the tag in the vehicle.

When a tagged vehicle approaches an instrumented bridge and the tag is within range of the transponder, the transponder will send a signal to the data acquisition unit on the bridge to activate the data storage. The transponder will read the vehicle identification number written on the tag and send its information and the bridge's response to a database.

The FBG interrogator will be powered on and will interrogate its FBG sensors continuously. Once an RFID tag has been identified, the transponder will send a signal to the data acquisition unit to begin data storage and transmission to the server. The data system will collect and record data for an allotted time

period. This system will provide controlled data collection because it is triggered by the presence of a tag in a permitted vehicle. It will also limit the amount of data to analyze because only data from permitted vehicles crossing the bridge will be collected. As the system develops, additional triggering features may be considered, for example, when a certain strain threshold is reached.

The data collected from the interrogator will be stored on an external hard drive. The extent of required storage space will depend on the duration over which data for a vehicle are recorded, the number of sensors on the bridge, the sensor scan rate, and the frequency of triggered traffic events. As the RFID development continues, the storage must be sufficient to store strain measurement data until cellular data transmission is established.

Data transmission will be implemented by means of a cellular module. The FBG strain measurements will be temporarily stored on an external hard drive, and then after the triggered event occurs, the database would receive the bridge response data. To provide a secure connection, Verizon Wireless recommended the Feeney Wireless Skyus and the Option Cloudgate as suitable options.

The data will be transmitted through the cellular network to the database. The RFID identification number assigned to the permitted vehicle at the weigh station with the axle loads and configuration will correlate with the same identification number recorded at the bridge site with the bridge response data. This would form a single case that contains the vehicle identification number, vehicle axle weights, vehicle gross weight, vehicle axle configuration, the time the vehicle passed over the bridge of interest, and the bridge strain measurement data. The vehicle load effects can then be associated with the measured structural response data obtained from the FBGs.

The database will work in conjunction with software to provide limited access to the combined vehicle and bridge information. Individuals, such as WYDOT bridge engineers, will be able to log into the database to view the most recent bridge activity. This software will allow the bridge owner to perform the necessary analysis procedures, whether they be load rating procedures, permitted vehicle hysteresis, or long-term monitoring to determine changes in bridge behavior.

5.1.2 Instrumentation Design

The instrumentation was developed in collaboration with an electrical engineer, Mr. James Branscomb. Field instrumentation necessary for the discrimination of bridge strain data based on identified permitted vehicles primarily relies upon a robust FBG sensor interrogator, Ethernet controller, data processing microcontroller, data storage module, cellular transmission module, reliable power source, RFID transponder, and RFID tags.

As discussed earlier, two Olimex mod-enc624J600 boards create the Ethernet to SPI data link from the interrogator and cellular network to the microcontroller. The boards' main components are Microchip's enc624J600 10/100 Base-T Ethernet controllers.

By using the Ethernet controller to form the SPI connection, the Atmel ATxmega64a3 microcontroller is able to receive continuous strain data from the FBG interrogator. The microcontroller allows the user to define which parameters will trigger the data storage of field measurements. As of now, the detection of an RFID tag is the trigger for storing the field test data.

As previously mentioned, two cellular modules, as advised by Verizon Wireless, were explored. A second Ethernet controller will be used to link the microcontroller and the cellular module. The purpose of the controller is to convert SPI signals back to the Ethernet so that the field strain data can be directed through the cellular network.

The current system development consists of a printed circuit board (PCB) containing two Ethernet controllers, microcontroller, programming port, voltage supply and regulator, LED indicators, and general purpose input/output (GPIO) pins to be used for future programming. Detailed descriptions of the PCB along with images are found in Danforth (2015).

Solar panels would be effective power sources for the RFID system for a few reasons. Bridges in Wyoming are often located in remote areas, so access to a power supply is limited. The Wyoming weather conditions often provide enough sunlight to power various electronic devices; for example, the variable speed limit signs use this technology. Also, solar panels are economically feasible and are practical to install.

The RFID system that triggers the microcontroller consists of three main physical components: an RFID reader, antenna, and tags. The CS203ETHER Integrated RFID reader both reads and writes information to the tags and transmits data. It is designed to withstand extreme weather conditions, including water and dust, with a high read rate. The RFID antenna communicates with the tags using radio frequency signals. The antenna has a range of approximately 9 meters; however, it can be coupled with an additional IP67 antenna for extended radio frequency range. The reader and antenna have thus far been referred to as the transponder, as they are physically enclosed in one unit that can be powered through an Ethernet connection.

The CS6710 Windshield RFID tags are each assigned a unique identification number, and they can store data transmitted from one transponder that can be read by another transponder at a different location. The tags are designed to be coupled with the CS203 integrated reader and placed on the inside of cars, buses, and trucks. The tags are passive, meaning they do not require batteries in order to communicate with the reader and antenna and are more economical than active tags that need batteries.

5.1.3 System Validation Procedure and Results

Field tests for the triggering mechanism validated the performance of the RFID system components. The validation procedure was considered successful when the RFID transponder recognized the presence of the RFID tag in an approaching vehicle, recorded the tag identification number, and triggered the storage of FBG strain data for a predetermined amount of time. This procedure was designed to test the system for a possible deployment project, so the focus was to demonstrate the capabilities of the triggering mechanism to provide a basis for future work.

Two operational modes were developed for the system: software and hardware. The software mode required use of a laptop computer that commands the microcontroller to store strain sensor data. This mode was utilized for field tests. Having a laptop in the field is not ideal because it cannot handle extreme weather conditions, requires additional space in a weatherproof enclosure, and calls for an increase in power supply. The hardware mode was developed to prevent this scenario, and if the hardware mode is used, the laptop is not needed in the field. The hardware mode was under development at the time of testing; therefore, the software mode was used for field tests. However, the hardware mode has since been systematically validated, and it will be functional for field tests in the future.

The RFID triggering tests were performed on Highway 17 (Roger Canyon Road) north of Laramie. The equipment was powered by means of a vehicle using a power convertor. Highway 17 has two lanes that are each 11-feet wide, unlike interstate lanes that are typically 12-feet wide. The distance from the edge of the lane to the transponder was 6 feet, and the distance from the ground to the bottom of the transponder was also 6 feet. The transponder was on the south side of the highway facing west. The RFID tag placed in the car was 5 feet above the ground.

The tests were organized so that the initial positioning of each RFID component was established prior to testing the system at full speed, including the position and direction of the RFID transponder, RFID vehicle, and RFID tag. For all tests, the vehicle was driven east toward the transponder. Each time the transponder detected the tag, the FBG strain data from three sensors were recorded for the allotted 30-second time frame.

The horizontal direction to which the transponder would detect the tag most effectively was determined by three different arrangements. The tag was placed in the upper left-hand corner of the windshield, and the vehicle travelled at 105 KPH (65 MPH).

First, the transponder was faced parallel to the oncoming vehicle, or straight toward the tag. This method was successful when the vehicle travelled in the closest lane; however, the transponder did not detect the tag when the vehicle was in the farther lane. Second, the transponder was directed perpendicular to the road. This angle was effective for the vehicle in the farthest lane; however, it did not trigger when the vehicle was in the closest lane. Third, the transponder faced the northwest direction at a 45-degree angle. When the vehicle was located in the closest and farthest lanes, the transponder identified the tag and triggered the data to be saved onto a file.

The position of the transponder from the ground also varied throughout testing. It was determined that the system was triggered occasionally at a height of 5 feet, consistently at 6 feet, and rarely at 7 feet. Clearly, this distance will alter depending on the height of the tag target for permitted vehicles in future testing. Additionally, the transponder was initially located at a distance of 8 feet from the edge of the lane; however, the distance was decreased to 6 feet for reliable triggering. The vertical angle that the transponder was directed was not tested because it is a feature that should be considered based upon the setup of the system in the future.

To determine the range from the transponder to the tag, the tag was placed in the upper left-hand corner of the vehicle windshield. The transponder was directed at a 45-degree angle northwest. The vehicle was located in the lane closest to the transponder and travelled at a speed of 16 KPH (10 MPH). The transponder detected the presence of the tag when the vehicle was approximately 3 m (10 ft) from the reader, measuring parallel on the road. The vehicle then travelled in the farthest lane, again headed east. With the tag farther away, the transponder detected the tag when the vehicle was in line with the reader.

The tags were designed to be placed on the inside of a vehicle's windshield. For the field tests, the tag was initially placed on the upper left-hand corner of the windshield. The vehicle was driven at 105 KPH (65 MPH) in the closest lane, and the transponder detected the tag six out of six times consecutively. The vehicle was then driven in the farthest lane with the same tag positioning, and the tag was identified in two out of four runs. As a result, an additional tag was added to the upper right-hand corner of the vehicle. The transponder then detected the tag two out of two times while the vehicle was in the farthest lane. This test suggests that the maximum perpendicular distance for consistent triggering is approximately 5.5 m (18 ft), and inconsistent triggering occurs at a distance of 8.5 m (28 ft) for a system using one antenna.

Up to this point, the positions of the transponder, vehicle, and tag were established, and the outcome of the three tested parameters had to be confirmed. The transponder was angled at 45 degrees facing the northwest direction; the vehicle was located in the farthest lane to test the worst-case scenario for vehicle placement; and the tag was placed in the upper right-hand corner of the windshield. The vehicle was driven at 105 KPH (65 MPH), and the transponder recognized the tag, triggering the data saving system six out of six times. These tests were sufficient to determine that the RFID triggering system functioned as intended.

After the vehicle event was triggered, the FBG strain measurement data were automatically saved to a file onto the computer hard drive. The file included the wavelength readings, tag identification number, date, and time, respectively. The wavelength readings were recorded from three of the four available interrogator channels, where one FBG was located on each channel. The sensors were not the focus of the field tests nor were they adhered to a host material affected by traffic events, so the readings fluctuated only slightly due to noise and marginal temperature variations.

6. LABORATORY VALIDATION

Task 4 was initially intended to validate tasks 1, 2, and 3 in the laboratory. However, it became feasible and more efficient to validate only task 1 in the laboratory and to prove the function of the systems developed in tasks 2 and 3 independently, as described in the foregoing chapters. To validate task 1, a laboratory model of a bridge was designed and constructed. The model bridge consisted of two girders that were vertically supported at four points resulting in a three-span continuous configuration. Utilizing a three-span design allowed for the measurement of bridge behavior undergoing positive and negative bending. In order to develop techniques for sensing both steel and concrete structures, one girder was constructed of a wide flange steel beam, and the other utilized a post-tensioned concrete beam.

The design of the experiment was loosely modeled after a three-span bridge on Interstate 80 between mileposts 310 and 311 west of Laramie, Wyoming. Analysis of this bridge provided some approximation of the magnitude of measurements that will be required of the resulting system. The field study will provide an opportunity to field test the methodology developed in this study.

6.1 Laboratory Model

The I-80 bridge that was modeled in the lab consisted of a three-span, continuous, non-composite steel girder design, utilizing W33x130 rolled-section girders spanning 12.3 m (40.5 ft), 15.4 m (50.5 ft), and 12.3 m (40.5 ft) for a total length of 40.1 m (131.5 ft). A girder-line model of this bridge was developed using SAP2000 (Computers & Structures, Inc 2011) finite element structural analysis software, and the model was analyzed for an HL-93 design truck, where it was assumed that one-half of each axle load would distribute to the beam-line, and no lane load was applied. Service-level loads were used to demonstrate that the SHM system will be capable of measuring the structural response of a bridge under elastic conditions. Based on this loading, the maximum curvature in the bridge was found to be 0.000942 m^{-1} (0.000287 ft^{-1}), corresponding to a maximum strain in the extreme fiber of the cross-section of 792 $\mu\varepsilon$.

The laboratory experiment was designed to achieve the same maximum strains as those determined from analysis of the I-80 highway bridge. Due to constraints on support locations for the laboratory bridge, the span ratio for the laboratory setup was modified slightly, and the laboratory beams spanned 2.7 m, 3.7m, and 2.7 m (9 ft, 12 ft, and 9 ft) for a total length of 9.1 m (30 ft).

A small cross-section rolled wide flange beam (W4x13) was used to form one girder for the laboratory bridge. A post-tensioned concrete beam was sized to produce approximately the same flexural rigidity as the steel beam while providing adequate strength to carry the required loads. The resulting section was a rectangular beam 15 cm (6 in) deep by 11 cm (4.5 in) wide. Use of a pre-stressed beam allowed the beam to undergo the desired curvatures for the experiment while still supplying adequate strength to carry the necessary loads.

Based on the flexural rigidity of the steel section, the load necessary to induce a strain in the extreme fiber of the section equal to that predicted by the analysis of the highway bridge mentioned above was calculated by scaling the loads according to the section depths and resulting curvatures. The scaling process resulted in load applied to the laboratory bridge roughly equal to 6% of the load on the I-80 bridge from the HL-93 design truck.

The load cart consisted of a concrete block, a concrete slab, two mounting beams, four load cells, and four non-swiveling V-notched casters. The concrete block was placed directly above the rear wheels. A

schematic of the load cart design is shown in Figure 6.1. Figure 6.2 shows the constructed laboratory experiment with the load cart, steel and concrete beams, and the support locations.

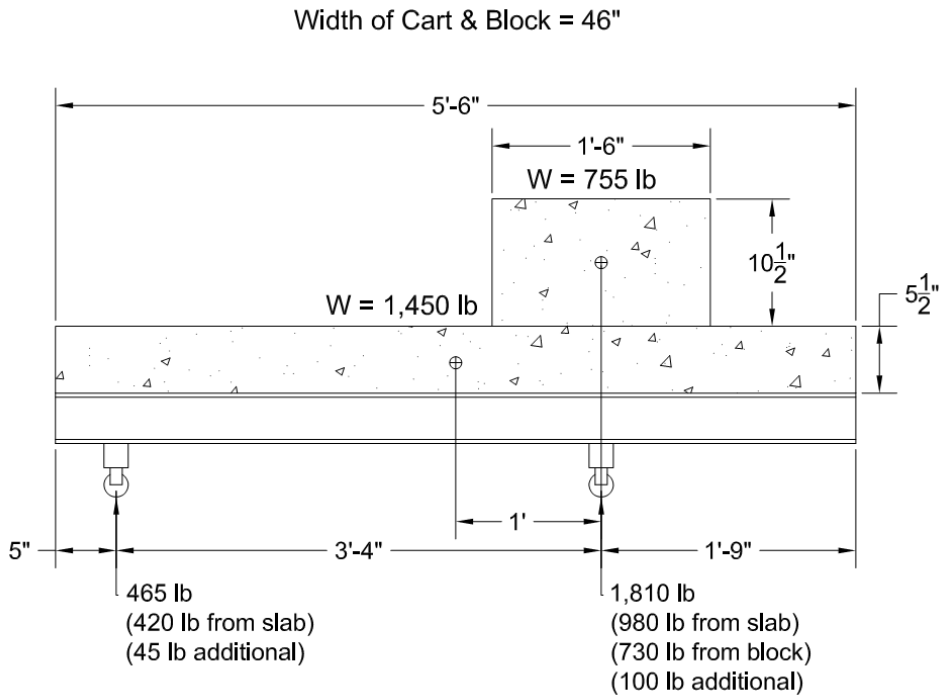

Figure 6.1 Schematic of Load Cart for Laboratory Test

Figure 6.2 Laboratory Test Setup

Fifty-six FBG sensors were installed on the beams for the laboratory experiment. For each beam, four sensors were installed about each beam cross-section at seven locations along the span of the beam. Figure 6.3 shows the sensor placement on the cross-section of each beam, and Figure 6.4 shows the locations of the sensors along the length of the beams.

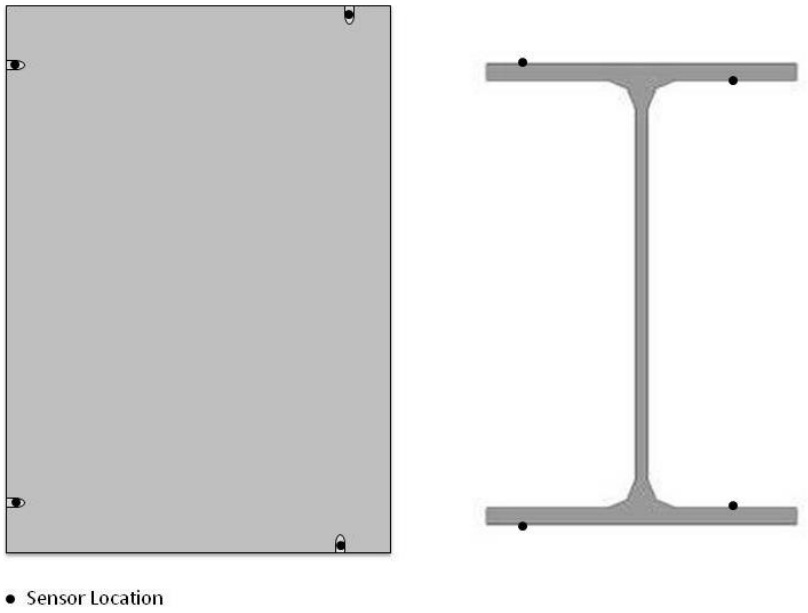

Figure 6.3 Sensor Locations on Beam Cross-Sections

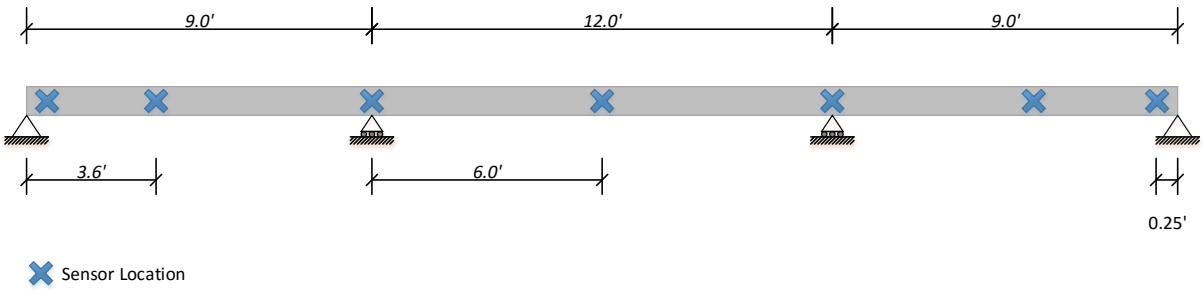

Figure 6.4 Sensor Locations Along Beam Length

On the cross-section of the beam, sensors were placed at the extreme fibers of the section for strong-axis bending to measure the curvature of the beam and the neutral axis depth. Measuring strain at the extreme fibers allows the strain sensors to read larger measurements for the same value of curvature.

Typically, three-span bridges achieve the maximum load effects due to bending over the supports, at mid-span of the middle span and at approximately 40% of the span in from the end supports on the exterior spans. This rule of thumb is reflected in the AASHTO LRFD Design Specifications (2012) in the section discussing the calibration of the HL-93 live load and load factors and was echoed in discussions with WYDOT officials regarding points of interest for curvature measurement. Therefore, these locations were selected to take measurements on the bridge. The sensors placed at the end supports allowed for the measurement of rotational fixity in the supports, and the sensors located between the supports aided in determining the stiffness parameters of the beam.

The span configuration was modeled in SAP2000, with a moving unit load used to determine the analytical curvature envelope for the laboratory structure. The maximum positive load effects in the first and third spans would have occurred near the sensors placed at the 1.04 and 3.06 span locations. According to the simulation, the curvature at the maximum locations in the exterior spans was 3.52% higher than the curvature at the sensor locations. For the middle span, the analytical model calculated that the maximum positive curvature would occur at the mid-span where the sensors were located.

The analytical models indicated that the maximum negative load effects would occur over the supports for the structure, as would be expected. Sensors were placed as near to the ends of the beams as possible to measure any curvature due to rotational fixity in the end supports. For the steel beam, sensors were placed within 5 cm (2 in) of the end. However, sensors on the concrete beam needed to be moved in approximately 20 cm (8 in) from the ends due to requirements for strain averaging and adhesive development length. Because the sensors in the tests were inset along the span due to interference from connections, they could only measure the moment near the ends of the beam, but not at the ends. However, as the analytical moment distribution was linear for the loading, the curvature at the end of the beam was found by linearly extrapolating from the values at the sensor locations.

6.2 Multiplexed Sensor System Design

For a multiplexed FBG system, a sensor plan should be carefully developed prior to installing any sensors to ensure that the operating wavelength spectrum of each channel of the interrogator is efficiently utilized. The operating spectrum of an interrogator is often the largest constraint on the number of sensors that can be effectively multiplexed, and interrogators with wider spectra or more channels will incur significant costs.

Therefore, consideration must be given to the wavelength range that multiplexed sensors will experience under operating conditions. If the reflected peaks from two FBGs on the same channel overlap during operation, interrogators cannot differentiate the light returning from the two sensors, and the reflected light will register as a single peak returning from a single FBG. This overlapped peak confuses the data collection and renders those sensors ineffective. This problem occurs if the unstrained FBG peaks are not spaced far enough apart on the wavelength spectrum to allow for the wavelength shift caused by the strain conditions.

The wavelength spacing can be adjusted by applying different magnitudes of pretension to the fibers while they are being adhered to the structure. Enough pretension can be applied to a fiber to cause a wavelength shift of about 4 nm without causing concern for over-tensioning the fiber during the FBG installation.

To prevent overlapping peaks, preliminary analysis of the expected structural behavior should be performed to determine the appropriate location and pretensioning necessary to place multiplexed FBGs with adjacent wavelengths. The maximum shift on the light spectrum will be dictated primarily by the maximum strain that the fiber will undergo while in operation. For a maximum strain of 0.003, the corresponding shift in wavelength is approximately 4 nm.

The maximum expected wavelength shift due to strain provides an estimate on the necessary spacing between wavelength peaks, but one must be judicious in spacing FBG wavelengths to also maximize the number of sensors that can be multiplexed onto a single channel. In areas of the structure where large strains are unlikely to occur, the wavelength spacing may be reduced. However, if two fibers possess adjacent wavelength peaks on the spectrum and are likely to experience concurrent opposing strains (one fiber undergoing positive strain, while the other experiences negative strain), bringing the wavelength

peaks toward each other, then the wavelength spacing between them should be increased appropriately. Care can be taken to place FBGs with adjacent wavelengths in areas of the structure that will undergo concurrent strains in the same direction, allowing for a reduction in the wavelength spacing.

A sensor plan that maps the locations of the FBGs on the structure with their corresponding wavelengths helps to design an effective layout for the FBG sensors that can efficiently utilize the operational spectrum of the interrogator. System designers must determine appropriate wavelength spacing for the strains expected in the structural locations being measured. A sample sensor plan, which was used in the laboratory experiment design, is provided in Figure 6.5. In the figure, sensor locations are indicated with the letter X and the four-digit numeral indicates the wavelength of the sensor in nanometers.

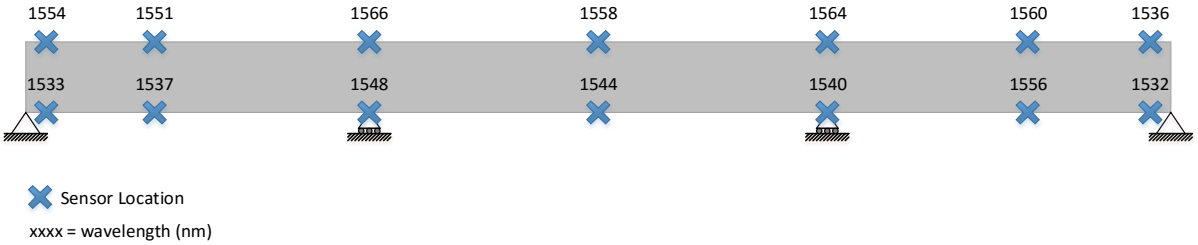

Figure 6.5 Sensor Placement for Concrete Beam

6.3 Temperature Compensation

FBG sensors are sensitive to changes in temperature and are not self-compensating for temperature variations. Therefore, it is necessary to separate the wavelength shift due to temperature variation from the wavelength shift due to mechanical strain in the host material. While the relationship between temperature and wavelength shift is well established, measuring temperature introduces complexity to the system. It is easier to measure the temperature effect on wavelength directly by using an FBG that is isolated from mechanical strain, and directly subtracting this apparent strain from the other bonded sensors on the structure to determine the resulting mechanical strain. The computations for this procedure are outlined in detail in Jung (2015).

To measure the thermal effect on FBG readings, it was necessary to develop a method for isolating an FBG sensor from mechanical strain while providing adequate protection to ensure durable operation. To achieve this, an FBG sensor was inserted into a protective heat shrinking tube, which is typically used for protecting splices in optical fibers. Using a heat source, one of the tips was heated until it shrank and secured a bond with the fiber. Then the fiber was compressed to induce a buckled shape inside the protective sleeve. Finally, the other tip was heated to lock the fiber into place while being careful to maintain the buckled shape. The resulting protective sleeve was pinched at the ends, and a gap remained in the middle to allow the sleeve to expand and contract as temperature fluctuates without inducing mechanical strain in the fiber.

6.4 Sensor Installation, Protection and Repair

In adhering the fiber Bragg gratings to bridges, care must be taken to ensure good strain transfer and reliable readings. The fibers need to be aligned along the desired axis of strain measurement, and it must be ensured that the fibers are securely attached to the host material without any slack or buckling in the fiber across the sensing region. Slack and buckling in the fiber are prevented by applying a slight pretension to the fiber while adhering it to the host element. While a nominal amount of pretension is necessary to ensure a sensor is installed straight and with a good bond, the specific amount of pretension

necessary will be dictated by the wavelength required by the sensor plan. Care must be taken not to over-tension the FBGs, as they can be brittle and have a tendency to break across the sensing region, which is slightly weakened during the manufacturing process (Li, Ren and Li 2012). Therefore, when ordering FBGs it is important to order sensors with base wavelengths that vary all across the effective spectrum of the interrogator.

Separate methods were developed for installing, protecting, and replacing FBG sensors for steel and concrete structures. The specific methodology is detailed in the following subsections.

6.4.1 Installation on Steel Elements

As steel is a homogeneous material, the strain sensor can be adhered directly to the region where measurement is desired. It was determined that adhering an FBG directly to the surface of steel elements using cyanoacrylate adhesive achieves satisfactory strain transfer. This was shown in previous work (Maurais 2012), where an FBG was adhered to a steel dog-bone specimen that was also instrumented with a traditional foil resistive strain gage and subjected to cyclic axial loading. The average discrepancy in strain measurements between the FBG and the strain gage at the peak load was 0.13%, demonstrating that this method of adhering FBGs produces strain readings comparable to commonly accepted practices for traditional strain gages.

The specific type of adhesive used for the installation procedure on this project was a thickened fast curing cyanoacrylate adhesive called Lightning Bond™, which comes with an activator spray that accelerates the curing process. Loctite™ produces a similar product. Applying the FBGs to the steel material with the proper pretension requires methodical precision. The method devised for achieving an adequate bond with the appropriate pretension is as follows:

1. Remove any mill scale or paint using a grinder or wire brush. Then clean the material surface, removing all oil, and slightly roughen it with sand paper.
2. Carefully mark the location to be measured on the element and draw a straight line along the axis of measurement. Then position the fiber along the axis of measurement so that the FBG region of the fiber is positioned at the location of interest. Tape one end of the fiber to the structure to aid in aligning the fiber for the next step.
3. Apply the cyanoacrylate adhesive approximately 5 cm (2 in) away from the sensing region along the axis of measurement. Set the fiber into the adhesive so the FBG is aligned and positioned correctly and spray the activator over the adhesive region to accelerate the curing process. Hold the fiber in place until the adhesive cures (about 30 seconds).
4. Once the adhesive has cured, apply the cyanoacrylate adhesive to the region to be measured ensuring a minimum adhesive length of 3.8 cm (1.5 in). Then, gently adjust the tension on the fiber until the target wavelength is achieved. Next, press the fiber against the steel so it is aligned with the axis of measurement and in good contact with the adhesive. Hold the fiber steady, ensuring that it is tensioned to the appropriate wavelength, and apply the activator to the adhesive. Hold the fiber in place until the adhesive cures (about 30 seconds). (As an alternative to manually holding the fibers in place while the glue cures, a pair of flat clamps or strong magnets may be used to hold the fiber in tension against the steel member. For this approach, the fiber should be protected from the clamps or magnets using a thin piece of rubber or similar cushioning material. Prior to applying the activator spray, verify that the pretension is stable by monitoring the wavelength for any change.)
5. Slowly release hold of the fiber while monitoring the wavelength for any significant drop in wavelength. If the wavelength of the applied FBG fails to stabilize at a higher wavelength than the base wavelength, then adequate bond has not been achieved. If a satisfactory bond is not achieved, refer to the subsequent repair procedure.

Variations on these methods were tried during the installation of sensors on the laboratory structure as the procedure was refined. The devised attachment method was generally effective. Of the 28 sensors installed on the steel beam, three experienced a loss of pretension greater than 25% between the time of installation and the time that the tests were performed. For the remaining sensors, the average pretension loss was 10%.

6.4.2 Protection on Steel Elements

For steel material it was decided that covering the fiber with a rugged, durable tape would be the simplest method for providing protection. The tape provides adequate protection and also holds the fibers in place. Fiber with the additional plastic protective coating should be spliced between FBG sensors to provide further durability under the tape. Various tapes were investigated for their bond quality, weatherproof capability, and ability to provide protection. A modified butyl rubber tape produced by Permatite™ was selected as the best option. It is rated for exterior exposure with a temperature range from -40°C to 121°F (-40°F to 250°F) and a watertight seal. The tape is approximately 3 mm (1/8 in) thick with a soft rubber-clay consistency, and it is available in various widths. The tape bonds well to steel, although no long-term environmental exposure tests were performed. The steel should be clean and free of mill scale and oil prior to applying the tape.

6.4.3 Repair on Steel Elements

If a fiber breaks on a multiplexed channel, then the signal from all FBGs beyond the break will be lost. The location of the last FBG reflecting a signal back to the interrogator can be used to locate the break in the optical fiber, as the break will be located somewhere between this last reporting FBG and the next sensor on the fiber. To replace the damaged fiber, at least one foot of the protective tape must be removed from each side of the break to allow enough slack in the fiber to perform a splice. In regions where the lead fiber is protected by the additional sleeve, the tape can be carefully removed with a putty knife. In regions where the fiber lacks this protective sleeve it will be difficult to remove the tape without breaking the fiber.

If the break occurs near a sensor, where a fiber cannot be repaired by simply splicing in an additional length of fiber at the break, the damaged fiber will need to be removed and replaced. Once the tape has been removed, a putty knife or a razorblade can be used to scrape off the old fiber and adhesive. Sandpaper should be used to re-clean and roughen the surface. Then the new FBG can be spliced and installed according to the preceding installation instructions.

6.5 Sensing Concrete Elements

6.5.1 Installation on Concrete Elements

The method developed and tested by Maurais (2012) and discussed above was employed to embed FBG sensors in the concrete beam. Based on those tests, a bond length of 60 mm (2.4 in) was deemed sufficient to achieve adequate strain transfer for fibers embedded at reasonable depths in saw notches 3 mm (1/8 in) wide and 3 mm (1/8 in) deep. While embedding the fibers in a notch provides a good mechanism for strain transfer, it does present some accessibility challenges for installing fibers with adequate pretension. Furthermore, the majority of high-strength epoxies require at least 24 hours to fully cure. This makes it impractical for the fiber to be held in place manually until the epoxy reaches full strength. Therefore, a procedure was devised to apply an FBG fiber into a notch with adequate pretension and hold it in place long enough for the epoxy to cure. The devised method involves installing a heat shrink protective sleeve on the fiber, which bonds to the fiber and provides a means to grasp and tension

the fiber. These protective sleeves can be affixed to concrete using cyanoacrylate. While this bond is not adequate for permanent installation in service conditions, it is sufficient to hold the fiber in place temporarily while the epoxy cures.

The protocol developed for installing FBGs onto concrete members is as follows:

1. Prior to splicing the FBG into the channel line, slide a heat shrink protective sleeve onto each side of the FBG approximately 13 cm (5 in) away from the center of the sensor. Being careful to keep the sleeve in place on the fiber, set each sleeve into the heating unit on the splicer to bond it into place. Once the sleeves are in place, the FBG fiber can be spliced onto other fibers or leads following typical procedures.
2. Carefully mark the location to be measured on the host structure and draw a straight line along the axis of measurement. Then, using a 3 mm (1/8 in) thick masonry blade, cut a straight shallow notch into the beam along the axis of measurement approximately 3 mm (1/8 in) deep and 30 cm (12 in) long.
3. Align the fiber with the notch and mark off the locations for the FBG sensor, the un-epoxied region (approximately 75-130 mm (3-5 in), the epoxied regions on each side [65 mm (2.5 in)], and the protective sleeves. Then using these marks as a guide, apply a thin layer of cyanoacrylate adhesive to one of the protective sleeves and position it in the notch. Ensure that it is in the appropriate position, and firmly press it down until the adhesive cures.
4. Using a small flathead screwdriver or similar tool, distribute the epoxy into the bottom of the notch, filling it approximately halfway up in the epoxied regions. Note: for sensors being installed overhead or on vertical faces, it may be necessary to wait approximately 10 minutes after mixing the two parts of the epoxy for it to establish adequate viscosity to prevent it from running.
5. Apply a thin layer of cyanoacrylate adhesive to the remaining unattached protective sleeve and to the corresponding region of the notch. Then, gently apply the appropriate pretension to the fiber and press the sleeve into the notch. Firmly hold the sleeve in place to maintain the pretension in the fiber. Then spray the activator on the cyanoacrylate adhesive and continue to hold the sleeve until the bond is secure.
6. Using the flathead screwdriver, fill the epoxy region to the top of the notch with epoxy, being careful not to damage the fiber. Then monitor the wavelength for any significant drop in wavelength. If the wavelength fails to stabilize above the base wavelength, it indicates an inadequate bond between the sensor and host material. If a satisfactory bond is not achieved, refer to the subsequent repair procedure.

This procedure was used for installing the sensors on the concrete beam in the laboratory structure. Of the 28 FBG sensors installed using this approach, three sensors experienced a loss of pretension greater than 25%, and the average pretension loss in the remaining sensors was 13%.

6.5.2 Protection on Concrete Elements

Affixing protective materials to concrete is more difficult than affixing to steel due to the rough surface, to which the tape does not adhere well. Two methods were developed to protect fibers attached to concrete elements. The first method requires a more intricate installation process, but results in a more permanent system. However, if for some reason an element in the SHM system breaks, all of the sensors on the channel must be replaced. To begin, a notch is cut the full length of the bridge, and each sensor must be installed so that the fiber lies within the notch for the full length of the bridge. To ensure that the optical fibers fit into the notch, the fibers between sensors must be measured out to be the same length as the notch between sensors, so that the fibers can be installed onto the structure with very little slack. Once all the sensors have been installed, the entire length of fiber for each channel is laid into the notch and covered with epoxy, except for the un-epoxied regions where FBGs have been installed. Over the un-epoxied regions, a thin 2.5 cm (1 in) wide cover plate, made of either plastic or metal, can be attached to

the concrete using epoxy to seal off the notch. This method results in a very durable, permanent system. However, the installation process is complicated by the necessity of having a taut fiber between sensors; and it can be cumbersome to saw a notch the full length of the bridge. Finally, if a problem is discovered in any of the sensors after the protection system is in place, then the entire line of sensors must be cut out, and new sensors must be installed.

The second method does not provide as robust protection; however, it is easier to implement, and it allows for repairs to be performed without replacing all the sensors on a channel. For this method, shallow, 30 cm (1 ft) long notches are cut at sensor locations, and the FBGs are installed according to the installation procedure. Between sensors the more durable fiber with a 900 micron protective sleeve is spliced leaving enough slack between sensors to maintain workability. A strip of clear spray paint is applied along the length of the element and allowed to dry in order to produce a smooth surface. Then the fiber is attached to the element using the butyl rubber tape discussed in the steel protection method section. The tape must be pressed firmly onto the concrete to ensure an adequate bond. If there is excess fiber, it can be wound into a loop and covered with butyl rubber tape. Care must be taken not to wind the fibers into too tight of a loop, which would result in a loss of signal. A diameter of about 5 to 7 cm (2 to 3 in) is acceptable. The butyl rubber tape can be installed over the notched regions where sensors are installed, or a thin cover plate may be epoxied into place to provide extra protection for the bare fiber in the notch.

6.5.3 Repair on Concrete Elements

If protection method 1 was used, and it is discovered that a sensor is not performing, then all the fiber will need to be removed from the notch, and new sensors will need to be installed. The epoxy may be removed using a file and similar hand tools, or it may be easier to recut the notch using a masonry blade. Once all the sensors are removed, new sensors must be installed and protected according to the previous instructions.

If protection method 2 was used, the butyl rubber tape can be gently removed from the structure using a putty knife. Care must be taken not to damage the underlying protective coated fiber. If the break occurred along the fiber between sensors, then the disjointed fiber ends can be stripped, cleaved, and spliced according to common practice. The fiber can then be re-adhered to the structure using a fresh strip of the butyl rubber tape.

If the break occurred at or close to the sensor, then the sensor will need to be replaced. If a cover plate was used, it should be removed by scraping the underlying epoxy away with a putty knife. Otherwise, the butyl rubber tape can be removed by gently pulling it back using a putty knife. Enough of the lead fiber should be liberated to splice a new FBG onto the channel. To remove the old sensor, the epoxy can be removed with a file, and the glued fiber protectors can be pried out using a flathead screwdriver. Once the old fiber is removed and the notch is cleaned, a new sensor can be installed according to the preceding instructions.

6.6 Experimental Procedures

Experiments were performed on each beam to compare the measured behavior of the structure with the predicted behavior from analysis. For each beam, three types of tests were performed: a static test, a pseudo-static (crawl-speed) test, and a full-speed test. These are typical of the types of tests traditionally performed in load rating tests for bridges. The static test provides the most reliable results, as there is less uncertainty about the position of the load, and any dynamic amplification is eliminated. The goal of the crawl speed test is to approximate the results of the static test with a less time-consuming method. Crawl

speed tests were performed in the lab to verify their accuracy. Dynamic test results are typically compared to static or pseudo-static tests in order to calculate a dynamic impact factor. This report focuses on the statics tests; details of the crawl-speed and dynamics tests are found in Jung (2015).

During each test, three parameters were measured: the location of the wheels, the magnitude of the loads applied by the wheels, and the strains measured by the FBG sensors. In order to correlate these data, a stopwatch was used along with the timer mechanism built into the data acquisition software. Each wheel of the load cart contained a 2-kip Interface© 1210AF load cell connected to a computer using a data acquisition unit connected through a USB port. A program written in Labview© was used to record the data from the load cells along with the time of the measurement.

In order to achieve a consistent load distribution during the tests, the cart configuration was modified to bear on three wheels rather than four. This was achieved by raising the height of one wheel on the cart until it was not in contact with the beam. The result was a load cart supported by three wheels, one on the measured beam and two on the non-measured beam. This configuration provided a stable system that could produce a single point load traveling down the beam of interest with more consistent load distribution than the original four-wheel configuration.

The sensors used in the laboratory experiment were 5 mm (0.2 in) FBGs in SMF-28 acrylate fiber with base wavelengths ranging from 1530 nm to 1566 nm. The FBG data were recorded using a two-channel SmartScan© interrogator. Each channel was connected to 14 multiplexed FBG sensors installed along the length of the beam. One channel was connected to the sensors oriented on the extreme fibers of the cross-section of the test beam. The other channel was connected to the sensors oriented on the inside of the test-beam cross section. The sample rate of the FBG data was set to 4 Hz, and the data were averaged to produce one data point per second. The averaging of the data was done to limit the quantity of data recorded during the test and to reduce the noise of the data collected.

For the static load test, the load cart was moved incrementally along the beam at 30 cm (1 ft) intervals for the entire length of the beam. At each interval, the load cart was held in position for approximately 10 seconds while measurements were recorded. The interval that the load was held stationary for data collection is referred to as a load condition. Six static tests were performed on each beam to test the repeatability of the results. In-depth analysis was performed for the load condition that induced the largest curvatures measured in each span: a point load at 1.2 m (4 ft), a point load at 4.6 m (15 ft), and a point load at 7.9 m (26 ft).

6.7 Experimental Results and Analysis

In-depth analysis was performed with the load positioned at three locations on each beam: at 40% of the first span (1.04), the middle of the second span (2.05), and 60% of the third span (3.06). The load effects and the structural response were calculated from the raw data at each point, and the structural properties of interest were calculated for comparison with values found through analysis. Multiple data points were collected while the load was held stationary at a single position. The data collected over the time that the load was held in position were averaged to produce a single average strain value for each load location used in the analysis. The raw wavelength measurements from the FBG sensors were converted to strain using Equation 1.

Equation 2 was then used to calculate the curvature at each position on the bridge using these strain values. By considering the strain at two different cross-section depths, Equation 2 eliminates the need for knowing the neutral axis depth to calculate curvature, assuming that the strain distribution is linear through the depth of the bending member.

$$\Phi = \frac{\varepsilon_T - \varepsilon_B}{d} \quad \text{(Eq. 2)}$$

where: ϕ = curvature
ε_T = strain in top sensor
ε_B = strain in bottom sensor
d = depth between top and bottom sensors

In order to calculate the analytical load effects for comparison with the laboratory measurements, a beam was modeled in SAP2000 with the flexural rigidity *EI* set to unity; nodes were placed at sensor locations, support locations, and load locations; a unit load was positioned at the appropriate location to replicate the load condition of the laboratory test; and the model was analyzed for the resulting moment. The supports were modeled to provide vertical and lateral restraint only. The values resulting from the simulation provided the moment function for a load at the location modeled. This moment function could then be scaled by the analytical flexural rigidity of the beam and the measured load magnitude to determine the analytical load effects, such as strains and curvatures, for a given load configuration.

6.8 Concrete Beam Results

The results from all six static tests were averaged to produce a curvature distribution for each of the three load cases that were analyzed in depth: a point load at the 1.04, 2.05, and 3.06 locations. In all three load cases, the analytical model predicted curvatures higher in magnitude than those measured during the tests, except at the beam ends, where the end-conditions assumed in the analytical model forced the curvature to a value of zero. The elastic modulus (*E*) used for the analytical concrete model was based on Equation 5.4.2.4-1 in the AASHTO LRFD Design Manual (2012). This equation does not account for the stiffness of the aggregate used. A direct test of the elastic modulus for the batch of concrete used to construct the beams would have given better results. However, due to a malfunction of the testing machine, reliable data were not available.

In order to determine a modulus of elasticity that better approximated the experimental data than the value calculated using the AASHTO equation, the analytical statical moment distribution was scaled by increasing the modulus of elasticity value to approximate the experimental curvature distribution. The resulting modulus of elasticity was increased by 32.3% from 4,031 ksi to 5,333 ksi. An additional analytical model was developed using this adjusted modulus of elasticity.

The curvature distributions calculated from the analytical model, the experimental data, and the adjusted modulus of elasticity analytical model for the load position at 1.04 location are shown for comparison in Figure 6.6. The figure shows that the analytical model curvature tracks closely with the experimental curves for the various sensors along the length of the beam. However, the analytical curve indicates greater curvature at all positions along the length of the beam.

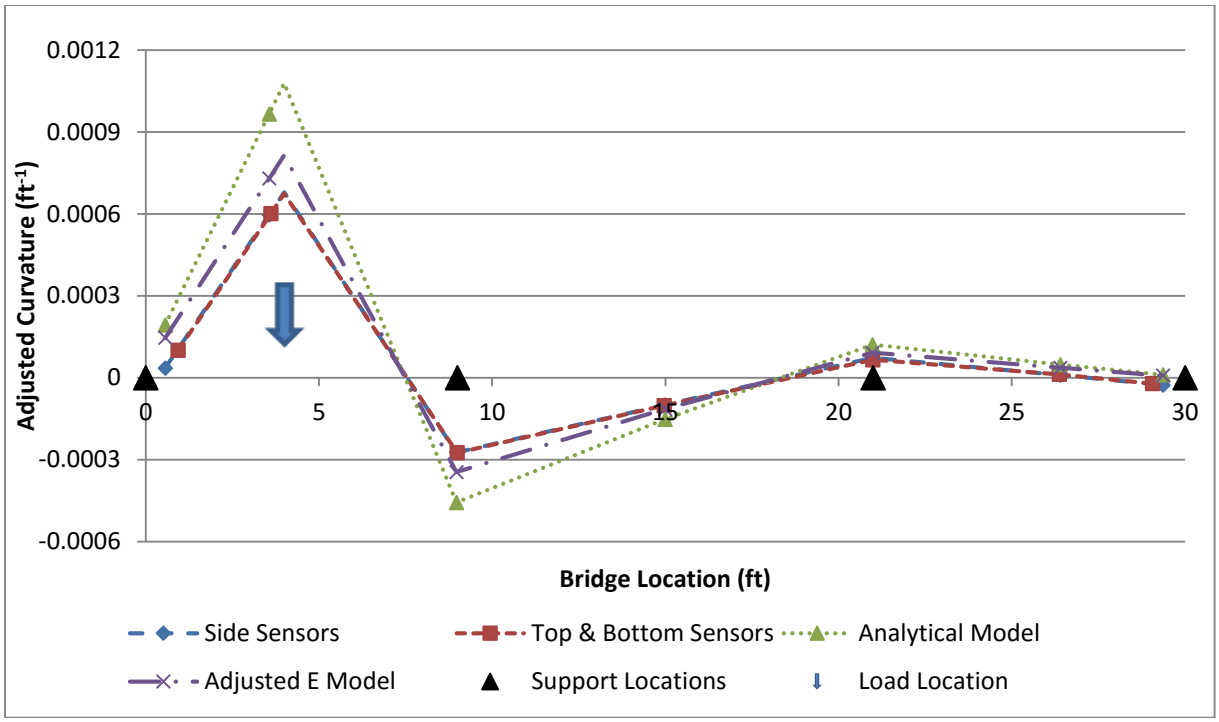

Figure 6.6 Comparison of Analytical and Measured Curvatures for Concrete Beam

6.9 Steel Beam Results

On the steel beam, there were significant discrepancies between the curvatures from the sensors placed at the extreme fibers and the curvatures measured by the sensors placed on the inside of the flanges. Figure 6.7 shows the average curvatures measured for the load positioned at the 2.05 location. The curvature for the inside sensors should have corresponded precisely with that for the outside sensors, as was the result for the concrete beam. However, in this case the inside sensors predicted higher curvature. For the three load configurations analyzed during the six static load tests, the average discrepancy between values measured by the two configurations was 30.5% of the mean value for the maximum positive curvature values and 29.3% of the mean value for the maximum negative curvature values.

Various factors may have contributed to the discrepancies in the measured values between the sensor configurations on the steel beam. The top sensors at the mid-support locations [2.7 m and 6.4 m (9 ft and 21 ft)] for both the inside and outside configurations experienced significant loss in pretension during the installation process. So they may not represent accurate results. Additionally, the strains in these locations may be affected by local bearing effects induced by the supports.

The curvature calculated from the top and bottom sensors on the same side of the beam were not equal in magnitude. However, there appears to be some correspondence in the strains measured by the inside top and outside bottom sensors, located near the top right and bottom left corners of the cross-section. Similarly, there is an apparent correspondence between the outside top and inside bottom sensors, located near the top left and bottom right corners of the cross-section. This symmetry could indicate the presence of out-of-plane bending, which would result in a rotation of the neutral axis. During the experiment, it was observed that the cart's wheel was bearing close to the edge of the flange rather than directly over the web. The beams constructed in the lab were not perfectly straight and the rigidity of the load cart may have pulled the steel beam toward the stiffer concrete beam, resulting in minor-axis bending. This notion

is consistent with observations from the neutral axis locations on the concrete beam. Furthermore, the eccentric load condition observed would result in a combined torsion and bending of the beam, which can result in secondary minor axis bending (Bremault, Driver and Grondin 2008). The minor axis bending would result in a tensile strain in both the top and bottom sensors on one side of the cross-section, and a compressive strain in the top and bottom sensors on the other side of the cross-section.

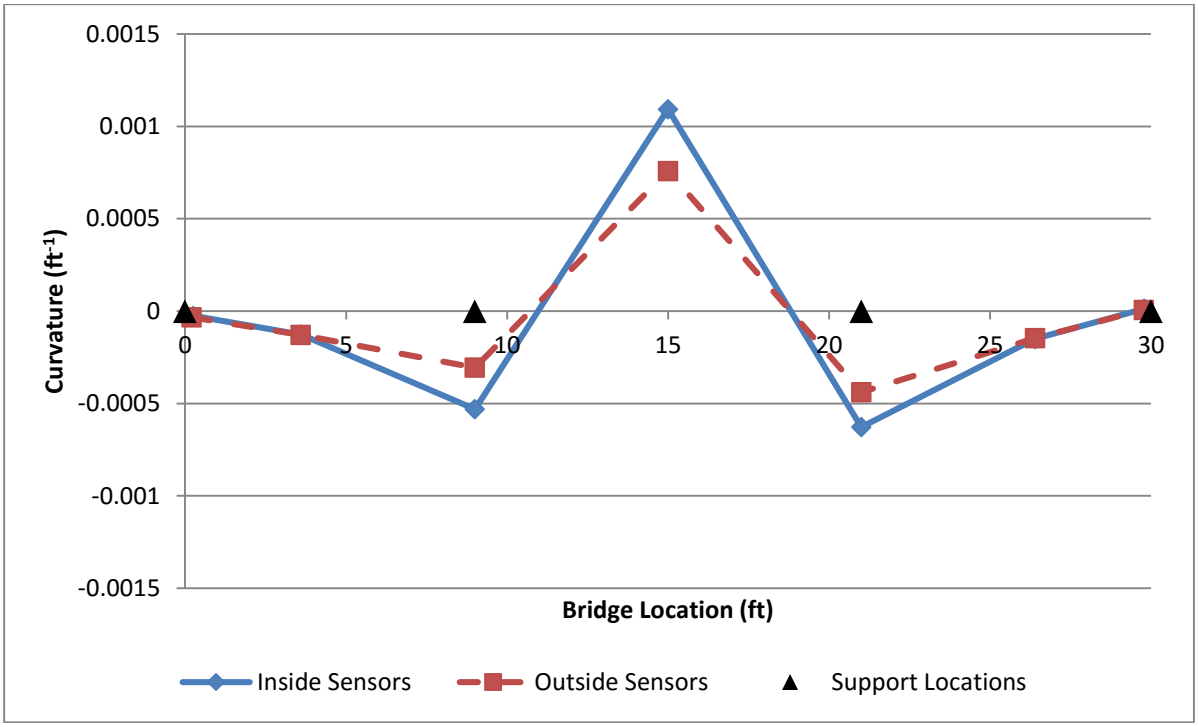

Figure 6.7 Curvatures Measured by Sensors on Steel Beam

Figure 6.8 compares the curvatures obtained from the sensors to the analytical values predicted by analysis of the steel beam subjected to strong axis bending for the load placed at the 1.04 position. In this case, the analytical model closely aligns with the curvatures predicted by the sensors in the experiment.

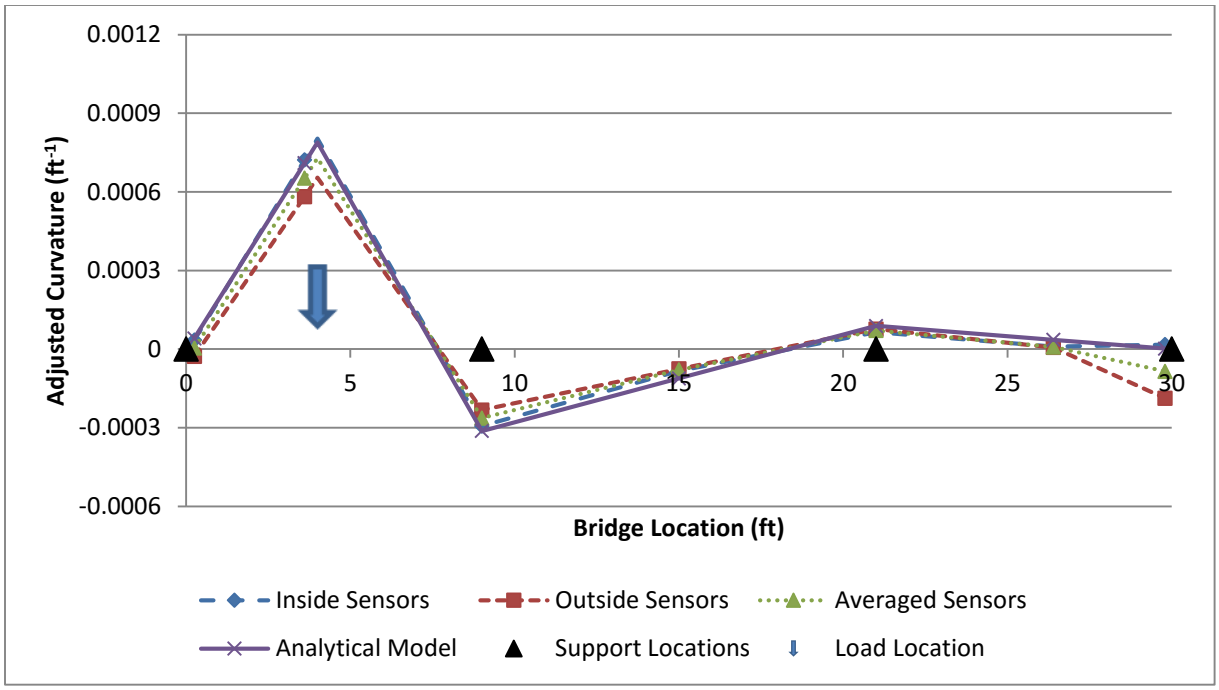

Figure 6.8 Comparison of Analytical and Measured Curvatures on Steel Beam

As previously discussed, the discrepancy between the measurements taken by the inside sensors and the outside sensors may be the result of secondary load effects like minor-axis bending. Averaging the measurements taken from all four sensors would have the effect of neutralizing these secondary load contributions on the data, as tensile strains on one side of the beam would be counteracted by compressive strains in the opposite side of the beam when the data are combined. The previous plot shows some of this behavior, where the averaged curvatures tend to approach the analytically predicted values. Additional discussion of the secondary load effects and the performance of the steel beam is found in Jung (2015).

7. FBG MICROBUCKLING IN COMPRESSION

Generally, FBG sensors are installed after some pretension is applied to the sensor. This process is intended to maintain a net tension in the sensor when compressive strain is applied. When an FBG is unstrained, it has a base wavelength that is determined when the FBG is created. For strain sensing applications, FBGs are typically pretensioned to a wavelength of 2 nm to 5 nm above the base wavelength, depending on the expected strains that the FBG will experience. Pretensioning ensures that the FBG will remain in tension when strained throughout its service life. For the applications in this research it was important to examine how the FBG performs in the compression zone without pretensioning. It was hypothesized that since the fiber is embedded in epoxy, it is restrained from buckling in compression and will therefore maintain functionality in its compression range.

To test the FBG compression range functionality, an un-tensioned FBG was surface adhered to a wood block with a 70 mm (2.8 in) bond length. A strain gage was also surface adhered to the block adjacent to the FBG sensor. Cyanoacrylate adhesive was used to bond both sensors to the block. The strain gage data were used for comparison to the FBG strain data during the compression test. Wood was selected as the host structure material because it is easily strained in compression. Two ramp loading tests were run and the strain differences between the two sensors were compared.

The wood block was loaded up to a maximum strain magnitude of about 0.003, which is the design strain limit for concrete. The FBG maximum compression wavelength shift experienced by the FBG was 3 nm below its base wavelength. The block was loaded twice and the results of each repetition averaged to demonstrate that the FBG only measured about 83% of the strain measured by the strain gage.

One possible reason for the strain sensing inaccuracy of the FBG is local buckling of the fiber when compressed. FBG fibers buckle very easily due to their thin silica-glass structure (Mohammad, et al., 2004). Accurate compression range sensing by embedding an FBG in epoxy has been achieved in previous studies but requires an epoxy with specific properties and a specific embedment configuration (Le Blanc, et al., 1994). It was found in previous studies that adequate thickness and stiffness of the epoxy that embeds the FBG to the host are essential in order to prevent local buckling of the FBG. Other techniques that utilize magnetic actuators or fiber-guiding systems have proven to be effective in preventing local buckling of FBGs, but are not feasible for strain sensing applications of structural members (Mohammad, et al., 2004).

8. FINDINGS AND CONCLUSIONS

A rise in the energy sector has resulted in a greater number of trucks travelling with overweight loads or non-standard vehicle configurations. State bridge managers are responsible for assuring safe and efficient routes for these permitted vehicle loads over bridges. As a result, bridge engineers are developing methods to quantify the actual capacities of in-service bridges, which are generally higher than the analytical analysis indicates. A field-tested bridge analysis can lead to improved load ratings or the removal of bridge postings, allowing permitted vehicles to travel through the state safely without costly detours.

The University of Wyoming team executed the following research tasks:

1. Develop optical-fiber packaging, installation, and protection mechanisms for implementation in harsh environments.
2. Develop a low-cost, compact, and energy-efficient instrumentation package for SHM of bridges using FBG sensors.
3. Develop data collection, processing, and transmission capabilities for the SHM network.
4. Validate the developments in tasks 1, 2, and 3 in a laboratory environment.
5. Study the behavior of FBG sensors subjected to compressive strains in excess of initial tensile straining.

Each of the research tasks achieved meaningful outcomes as described in the following.

8.1 Task 1

Fiber Bragg Gratings have been used in various fields for decades; more recently, they have been introduced into the structural engineering field. FBGs are more commonly replacing TGs for field testing bridges. Regardless, some engineers are skeptical of replacing the TGs. To re-establish confidence in the performance of FBGs and to understand and describe the installation process for future possible deployment, the University of Wyoming used TGs to verify FBGs.

8.1.1 FBG Sensors Mounted on Concrete

Both experimental and finite element methods were used to determine the elasto-mechanical behavior of FBG sensors attached to a concrete host. The conclusions drawn from the FEA and the experimental tests relate primarily to the strain measurement accuracy of the FBG sensors bonded to concrete in notches. It was found that the FEA slightly over-predicts the strain transfer to the FBG when compared with test results. This conclusion is supported by the fact that for 80% of the configurations compared, the FEA strain transfer results were 1% to 9% greater than those seen in the experimental tests. Despite the FEA over-prediction, it is still possible to conclude there are some configurations that provide full strain transfer and some that do not. Before more detailed specifications can be made about which configurations are most effective, it is important to consider the feasibility of field implementation. Several issues such as the equipment, time, and level of installation complexity required for field applications must be evaluated.

After several laboratory and computer simulations of the FBG embedment procedure, it was concluded that the equipment and materials required to install an FBG in a notched concrete structural member are effective and obtainable for an engineering or construction crew. The embedment notches can be cut in the concrete with a masonry saw or formed as the concrete is placed. The Ultrabond 1300 epoxy was

effective because of its short cure time and availability; however, for overhead or vertical applications, a more paste-like adhesive with higher viscosity would be optimal.

The process of embedding an FBG in a concrete notch is fairly straightforward and feasible for field applications. After a notch is formed or cut into a concrete structural member, a thin layer of adhesive is placed in the bottom of the notch. An FBG is then placed onto the first layer of adhesive followed by a second layer of adhesive that covers the FBG and fills the notch. The specified adhesive cure time should be allowed before strain monitoring begins. The FBG embedment process takes less than 20 minutes per sensor, excluding the adhesive cure time.

An evaluation of the strain transfer test results reveals minor differences between the FEA and the experimental tests. The slightly lower strain transfer seen in the experimental results is attributed to several influential factors. One is the assumption of perfect bonds between the adhesive and the concrete as well as between the adhesive and the fiber in the FEA. This assumption is unrealistic in real conditions and resulted in greater strain loss in the experimental tests. Additionally, the form oil on the surface of the concrete prisms was not fully removed before applying the epoxy, possibly resulting in a softening of the concrete-epoxy bond interface. The size of the aggregate in the concrete may have also affected the strain sensing of the FBG. The maximum aggregate diameter was 20 mm (0.8 in), which is twice the length of the FBG sensor region. If the FBG sensor region was adhered directly over a single piece of aggregate, the strain measured by the FBG would have been more representative of that piece of aggregate rather than the prism as a whole. The conventional strain gage had a sufficiently long sensor region; however, electrical noise and sensitivity level are two parameters that may have affected the accuracy of the strain gage when compared with the FBG strain measurements.

Non-uniformities in the epoxy and the notch shapes may have also caused variations in the strain transfer in the experimental tests. The concrete notches were not formed in the concrete exactly as they were modeled in the FEA. There were imperfections such as air bubbles and non-exact geometries in the concrete notches that could have contributed to the difference in strain transfer between the FEA and the experimental tests. The epoxy may have also had air bubbles or long-term shrinkage behavior that influenced the strain measurements of the embedded FBG. Despite the various factors that affected the strain sensing accuracy in the experimental tests, good correlation between the physical tests and the FEA data was seen. The differences in strain transfer (1% to 9%) between the FEA and experimental tests for the five configurations compared were reasonably low. The FEA was, therefore, considered an effective tool for analyzing the FBG notch embedment strain sensing method.

The FEA results supported several conclusions about how the configuration parameters affect the strain transfer for the notch-embedment sensing method. One conclusion is that as epoxy bond length increases, so does the effective strain transfer length for a given configuration. This trend is true for all bond layer thicknesses and epoxy moduli. A second conclusion relates to the effect of epoxy elastic modulus on strain transfer. It was observed that strain transfer increases with an increase in the adhesive elastic modulus. This trend supports the conclusions of previous studies, which suggest that the closer the elastic modulus is to the concrete, the better the strain transfer.

The results of this study revealed an inverse relationship between bond layer thickness and strain transfer. It is seen that smaller bond layer thicknesses provide greater strain transfer. Additionally, the effect of bond layer thickness appears to have more of an impact on the V-notch configuration than the saw-notch configuration. This behavior is likely because the V-notch is wider with a tapered shape while the saw-notch geometry is narrower and more uniform. The bigger V-notch provides a greater volume of epoxy for strain loss to occur in. The tapered V-notch shape provides more epoxy between the FBG and the concrete than the saw-notch as the bond layer thickens.

The results also suggest that the saw-notch provides better strain transfer than the V-notch. It is expected that the configuration with the smaller bond layer thickness will provide enhanced strain transfer. It is seen, however, that the saw-notch configuration with a 3.2 mm (0.126 in) bond layer thickness provides better strain transfer than the V-notch configuration with a smaller 1.75 mm (0.069 in) bond layer thickness. In other words, even though the FBG is farther away from the host structure in the saw-notch than in the V-notch, the saw-notch still provides higher strain transfer. This implies that the saw-notch will provide better strain transfer than the V-notch in any situation where the epoxy modulus, epoxy bond length, and bond layer thickness are the same in both notch types.

The experimental test results also offer some insight toward what configurations will provide effective strain transfer in field applications. Results show a nearly fully developed experimental strain transfer value of 0.98 for the V-notch configuration with a 2.7 mm (0.106 in) bond layer thickness and a 30 mm (1.18 in) epoxy length. This implies that any V-notch configuration with an epoxy length of 30 mm (1.18 in) or greater with a bond layer thickness of 2.7 mm (0.106 in) or less will have a strain transfer rate of 0.98 or greater. This conclusion also applies to the saw-notch configuration since it was found that the saw-notch provides better strain transfer than the V-notch. A final conclusion is that decreasing the epoxy length and increasing the bond layer thickness will decrease strain transfer as seen with the 4.2 mm (0.165 in) bond layer thickness configuration.

8.1.2 FBG Sensors Mounted on Steel

The FBGs and TGs were installed on an S3x5.7 steel beam. There were six of each type of sensor, where one FBG and one TG were located in six different locations on the beam. The averaged results from each FBG and TG set at the various locations were compared for the six tests. The modulus of elasticity values was used for comparison because the averaged results were linear, so one slope value accurately represented the data set.

Set 1 had an FBG and TG located at the extreme compression fiber. At this location, the TG results were 11.3% higher than the FBG results. Set 2 was located on the underside of the top flanges with FBG results 14.8% higher than the TG results. Sets 3 and 4 were installed on the web of the beam on the same side at a 45-degree angle to record shear strain results. Set 3 FBG results were 8.8% higher than TG results while set 4 showed FBG results 14.2% higher. Set 5 was located on the top of the bottom flanges and the FBG results were 20.3% higher than TG results. Lastly, set 6 was mounted on the bottom of the bottom flange; the FBG resulted in an average of 2% higher than the TG results.

The FBG results based upon the six tests were within an acceptable range of the TG results. Set 5 is an exception that displayed unusual results, possibly due to an epoxy bond failure. Many assumptions were made for the verification tests that could explain the strain measurement discrepancies. Assumptions include a perfectly flat, sanded, and clean surface; flawless sensor application, resulting in a perfect bond; reliable foil gage measurements; exact angle alignment of sensors at 45 degrees and sensors parallel to each other; the beam stays within its elastic range; and that a difference in strain due to the distance between sensor sets is negligible. Although the assumptions represent ideal testing conditions, this is rarely the case.

Given the assumptions of the tests and additional test properties, the results are within a reasonable range. Typically, when comparing strain gages on the market to foil gages through laboratory testing, strain results within 5% are a reasonable expectation. Set 6 displayed this comparison with a 2% difference. However, based upon the assumptions and additional test properties, results within 15% are acceptable.

8.2 Task 2

Upon study of the market for commercially available instrumentation, particularly FBG network interrogators, it became evident that a commercial product was superior to anything that could be developed individually. Commercial products provide the low-cost, compact form-factor, and energy efficiency required for this project. Additional pursuit of custom instrumentation would have been a waste of research time and funding. Consequently, a two-channel SmartScan 02 Lite FBG interrogator developed by Smart Fibres was purchased for the laboratory study. This approach assured that the laboratory instrumentation conformed to the latest industry standards and had the reliability and durability to perform as required. The only other resources required in the laboratory are a standard Windows-based desktop computer and an Internet connection.

Selection of instrumentation for field application was merged with task 3 in order to successfully integrate commercially available hardware with a custom-designed microcontroller. Findings and conclusions for the instrumentation intended for field application follow.

8.3 Task 3

Future field deployment and operation of the SHM network emphasized proof of concept of the RFID triggering system for data collection and data storage capabilities. The research was focused on permitted vehicles. Additionally, the system was designed to correlate known vehicle data with the measured response of a bridge. The work focused on the RFID systematic description, the validation procedure, and the validation results for the proof of concept field tests.

The RFID system utilizes a transponder that wirelessly transmits data to and receives data from the RFID tags. RFID transponders will be installed at a weigh station at a Wyoming port of entry and at the bridge of interest. At the port of entry, the permitted truck information, including the axle weights and configuration, will be assigned to an RFID tag with an identification code that would be placed on the windshield of the vehicle. Another transponder placed near the bridge will detect the presence of the RFID tag and trigger the system to store the bridge strain data when the tagged permitted vehicle passes over the bridge.

Mr. James Branscomb was the primary developer of the instrumentation for the RFID triggering system and the microcontroller that drives the FBG interrogator. For the proof of concept testing, the triggering mechanism, data collection, and data storage were the specific parameters tested. The proof-of-concept tests were organized so that the initial positioning of each RFID component was established prior to testing the system at full speed, including positioning of the RFID transponder, RFID tag, and RFID vehicle. Each time the transponder detected the tag, the FBG strain data from three sensors were continuously recorded for the allotted 30-second time frame.

The proof-of-concept for the RFID triggering system was successful. It was determined that the success of the triggering is dependent upon the position of the tagged vehicle; the transponder, including the height and horizontal position; and the tag location in the vehicle. The proof-of-concept tests provided admissible results that were sufficient to move on to the next phase of instrumentation design and testing.

8.4 Task 4

The sensors installed on the concrete beam using methods developed in task 1 provided measurements similar to, but lower in magnitude than, what was predicted by the analytical model. It was necessary to account for averaging effects caused by the long gauge sensor configuration. Further discrepancies between the test results and the analytical model could be explained by a difference between the predicted and the as-built modulus of elasticity for the concrete.

The measurements taken on the steel beam were similar in magnitude to the values predicted by the analytical model. However, the measurements taken at different locations on the beam cross-section varied significantly where they should have been similar. This variation could be explained by the presence of secondary load effects induced by an eccentricity in the load on the beam that was observed during the experiment. In a few locations on the steel beam, the sensors experienced a significant loss in pretension after installation. The wavelengths from these sensors did stabilize at a point that indicated there was still adequate pretension to make the necessary measurements. However, the resulting measurements at these locations appeared inconsistent with measurements taken from other sensors during the tests. This may be due to an inadequate bond between the sensor and the beam. However, these sensors were located directly above the mid supports of the beam. So, the inconsistent measurements may have been the result of unpredicted localized effects from the supports.

Analysis of the curvature did not yield values similar to the analytical model. Comparing the measured experimental values with different hypothesized properties and loading scenarios on the analytical model allowed for reasonable postulations of the behavior that may have induced the recorded test data. The sensor data appeared to be significantly influenced by local effects at the support locations. Therefore, placing sensors directly over the support locations should be avoided. It may be necessary to offset the sensors a distance away from the support locations to minimize the influence of local bearing effects.

The curvatures measured by the sensors located at the extreme fibers of the concrete beam cross-section were similar to the curvatures measured by the sensors inset from the edges of the beam cross-section. This similarity in results supports the conclusion that the FBG sensors do not need to be located at the extreme fibers of the cross-section in order to measure accurate values. The neutral axis height values indicated that locating sensors near the sides of the cross-sections may incur unanticipated load effects due to minor-axis bending.

The sensors at the four locations on the steel beam cross-section each reported different magnitudes of curvature. It was postulated that this variation in results was caused by unanticipated secondary load effects such as minor-axis bending and torsional warping, based on observations of the load condition during the experiment. The presence of these incongruent curvature values makes it difficult to confirm that sensors located on the inside of the cross-section can accurately measure major-axis bending effects.

The presence of FBG sensors at multiple locations on the beam cross-section enabled the sensing system to detect discrepancies that were likely due to secondary load effects. To improve on the sensor arrangement used during these tests, sensors could be placed at the top and bottom of the beam cross-section along the minor neutral axis in addition to near the side of the beam. The sensors on the minor neutral axis would provide a more direct measure of the major-axis bending, and could be compared to the measurements taken near the sides of the cross-section to quantify secondary load effects.

The calculated load effects from the laboratory tests on the concrete beam are compared with the values predicted by an analytical model based on common structural analysis and bridge design practices. The measured curvatures from the laboratory tests were consistently lower than those predicted by the analytical model. It was postulated that the modulus of elasticity of the laboratory beam was higher than what was assumed in the analytical model. Lack of additional experimental data makes it impossible to confirm several of the foregoing explanations.

8.5 Task 5

Based on the findings in the literature and additional testing with steel specimens in this research, it can be reasonably concluded that effective strain transfer in compression can be achieved with proper bonding technique. Whether the ineffective transfer with the wood block specimens was a consequence of micro-buckling or some other phenomenon remains unknown, but also irrelevant. The important finding is that FBG sensors can indeed perform accurately when subjected to compressive strain.

9. IMPLEMENTATION RECOMMENDATIONS

The research and development reported herein lays the groundwork for continued study involving field deployment of the FBG-based SHM system. The essential elements of the system are in place. These elements include the following:

- Sensor installation and protection techniques for both concrete and steel host structures
- Commercial and special-purpose instrumentation for interrogating the SHM network
- A novel triggering system based in RFID technology to control the amount of data that are collected from the SHM network.

Subsequent deployment of the system on a bridge in the WYDOT inventory will require additional development of data storage and transmission capabilities, which will be particular to the location and characteristics of the targeted bridge. In addition, the objectives of the SHM network (such as observing the impacts of overweight and other permit vehicles, validating load-rating software, monitoring long-term health of the bridge, etc.) will dictate the nature of the sensor installation, the type and volume of data collected, and the required post-processing requirements. Hence, development of a general performance specification for real-time data analysis is not feasible. Rather, researchers engaged in Phase II of this study must coordinate with bridge engineers at WYDOT to identify a spectrum of SHM applications and objectives, for which individual data analysis techniques can be developed. Subsequent design and implementation of software to execute such data analysis will be needed to relieve bridge engineers from the burdensome and tedious tasks of sifting through raw SHM data streams themselves.

In addition to the general recommendation above to move toward field deployment of the SHM system, the following specific recommendations are offered.

1. Special attention should be taken when purchasing FBGs. Knowledge about existing technologies and manufacturers will help to assure accurate, consistent, and reliable strain sensor results. Particular points of interest include the wavelength range that can be sensed by the interrogator and the required spacing between central wavelengths of FBGs on an individual channel. The interrogator range and the spacing determine the number of sensors that can be installed on a single optical fiber.
2. In design of the sensor network for a particular bridge, sensors should be placed at a sufficient distance away from the neutral axis to ensure they are measuring meaningful flexural strain values. For many structures, the concrete deck will act integrally with the primary structural elements. This composite behavior (intended or otherwise) will shift the neutral axis toward the deck. Analysis should be performed for each structure to determine where the expected neutral axis will occur, and the neutral axis location should be considered when deciding where to locate the sensors on the cross-section.
3. A two-sensor configuration makes it difficult to distinguish any contribution from out-of-plane bending. If a sensor is located on a location of the cross-section where strains from one load effect act counter to strains from another load effect, these readings would underestimate the response of the structure to the loading. If these values were used to load rate a bridge, they would overestimate the capacity of the bridge. Placing the sensors close to the minor neutral axis of the beam would minimize the contributions from these secondary load effects. However, if there are significant secondary load effects, it would be important to consider them and the interaction of the stresses.
4. While the top flange of a girder is typically braced by the deck, the bottom flange often carries lateral loads along the girder line through bending until they reach a lateral brace that will transfer the loads into the deck (AASHTO 2012). The significance of these lateral loads should be investigated as part of the design process for the sensor network.

5. The SHM system will be capable of recording massive amounts of data. It will be necessary to develop methods to automatically decipher which data are significant and should be transmitted and saved by the system. An algorithm to save data with readings that exceed a certain threshold or the maximum response each day may be appropriate. Taking a relaxed-state reading each day may be appropriate for documenting changes in the structure or to verify the functionality of the sensing system.
6. Since trucks pass over a bridge in a matter of seconds, it is highly unlikely that significant effects of temperature change will occur during the load event. Hence, when the data acquisition system is triggered by the RFID signal, initial relaxed-state scans of the bridge can be used to establish a baseline of strains immediately prior to and perhaps after passage of the permitted vehicle. Such an approach effectively embeds temperature compensation in the software that drives data collection rather than in special-purpose sensors, which require additional cost and bandwidth in the interrogator.
7. The RFID triggering system requires additional development. Developments include the port of entry system installation, firmware advancement, larger transponder range capabilities, cellular data transmission capabilities, database establishment, and software formation. For instance, use of the E-ZPASS system, common in many states, could simplify application of the system at the port of entry, since it is already familiar to DOT officials and the trucking industry alike.
8. A database should be established that can manage a large amount of vehicle and bridge information and can be accessed by approved personnel, for example, WYDOT bridge engineers. Software as well as algorithms for automatic post-processing must be developed. One company that has been researched, Chandler Monitoring Systems, Inc., has developed some of these processes, and it may be worthwhile to pursue its guidance or services.
9. Port of entry sites would do well to couple weigh-in-motion systems to an RFID triggering system to automate collection of vehicle characteristics. Utilizing a static WIM system that already exists at the port of entries, bridge engineers can correlate that load to the bridge responses induced by permitted live loads.
10. Another possible enhancement to the SHM system could be a continuous load-rating system for permitted vehicles. Over time, a standard baseline could be built for specific permitted vehicles and bridge families. Instead of relying on a conservative analysis completed by BRASS-Girder, the actual responses would be measured and monitored for a variety of applied vehicle configurations. Algorithms and procedures would need to be developed to determine real-time bridge load ratings from bridge measurement data. By continuously monitoring the bridge, bridge management officials could potentially determine practices to safely increase the load ratings.
11. The SHM system could assist in identifying illegal loads and notifying law enforcement. Individuals or companies with overweight or oversize vehicles might not file for a permit in an attempt to bypass permit fees. Strain-level triggers implemented in the sensing network, coupled to RFID tags in trucks entering the state, could be used to detect and identify illegal loads.

REFERENCES

A.G. Lichtenstein and Associates, Inc. 1998. “Manual for Bridge Rating Through Load Testing.” *National Cooperative Highway Research Program Research Results Digest* (Transportation Research Board) (No. 234).

AASHTO. 2012. *AASHTO LRFD Bridge Design Specifications.* Washington, D.C.: AASHTO.

Annamdas, Venu Gopal Madhav (2011). “Review on Developments in Fiber Optical Sensors and Applications.” *IJME International Journal of Materials Engineering:* 1-16. Scientific & Academic Publishing.

Ansari, F., & Libo, Y. (1998). “Mechanics of Bond and Interface Shear Transfer in Optical Fiber Sensors.” *Journal of Engineering Mechanics,* 385-394.

Ansari, F. (2007) “Practical Implementation of Optical Fiber Sensors in Civil Structural Health Monitoring.” *Journal of Intelligent Material Systems and Structures*, v.18: 879-889, August.

Baez, Michael (13 May 2014). "Phase II." Message to McKenzie Danforth. Personal communication.

Barker, Michael, Cory Imhoff, Travis McDaniel, and Troy Frederick. 1999. *Field Testing and Load Rating Procedures for Steel Girder Bridges.* Jefferson City, MO: Missouri Department of Transportation.

Branscomb, James (Mar. 2013-Oct. 2015). Electrical Design Engineer. Wyoming Department of Transportation. Personal communication.

Bremault, Dennis, Robert G. Driver, and Gilbert Y. Grondin. 2008. *Limit States Design Approach for Rolled Wide Flange Beams Subject to Combined Torsion and Flexure.* University of Alberta.

Cardini, A., and J. DeWolf. 2008. “Long-term Structural Health Monitoring of a Multi-girder Steel Composite Bridge Using Strain Data.” *Structural Health Monitoring* 47-58.

Chajes, Michael, Harry Shenton III, and Dennis O'Shea. 2000. “Bridge-Condition Assessment and Load Rating Using Nondestructive Evaluation Methods.” *Transportation Research Record.*

Chan, T.H.T., L. Yu, H.Y. Tam, Y.Q. Ni, S.Y. Liu, W.H. Chung, And L.K. Cheng (2005). “Fiber Bragg Grating Sensors for Structural Health Monitoring of Tsing Ma Bridge: Background and Experimental Observation.” *Engineering Structures* 8.5: 648-59.

Computers & Structures, Inc. 2011. “SAP 2000 Version 15.”

Danforth, McKenzie. 2015. *Laramie River Bridge Load-Testing Plan with Sensor Verification and RFID Feasibility of Permitted Vehicles.* Thesis, Laramie, WY: University of Wyoming.

Doornick, J. D., Phares, B. M., Wipf, T. J., & Wood, D. L. (2006) “Damage detection in bridges through fiber optic structural health monitoring.” *Photonic Sensing Technologies, Proc. Of SPIE*, v. 6371, 637102-1 – 637102-12

Farhey, Daniel N. 2005. “Bridge Instrumentation and Monitoring for Structural Diagnostics.” *Structural Health Monitoring* 301-318.

Guemes, Alfredo, and Julian Sierra-Perez. 2013. “Fiber Optic Sensors.” In *New Trends in Structural Health Monitoring*, by W. Ostachowicz, 265-316. Udine: International Centre for Mechanical Sciences.

Heininger, Hilmar. 2009. “Research proposal, Faseroptische Sensoren zur Bauwerksüberwachung.” Mannheim Germany.

Jung, Michael, 2015. *Development of a Fiber Optic Based Load Testing System for Highway Bridges.* Thesis, Laramie, WY: University of Wyoming. December

Kreuzer, M. (2007) Strain Measurement with Fiber Bragg Grating Sensors, HBM, Darmstadt Germany, July 16, http://www.hbm.com

Kuang, K. S. C., M. Maalej, and S. T. Quek (2006). "Hybrid Optical Fiber Sensor System Based on Fiber Bragg Gratings and Plastic Optical Fibers for Health Monitoring of Engineering Structures." *Smart Structures and Materials 2006: Sensors and Smart Structures Technologies for Civil, Mechanical, and Aerospace Systems* 6174.

Le Blanc, M., S. Y. Huang, M.M. Ohn, and R. M. Measures. (1994). Tunable chirping of a fiber bragg grating using a tapered cantilever bed. Electronics Letters.

Li, Dongsheng, Liang Ren, and Hongnan Li. 2012. "Mechanical Property and Strain Transferring Mechanism in Optical Fiber Sensors." In *Fiber Optic Sensors*, by Dr. Moh Yasin, 439-458. Shanghai: InTech.

Matta, F, F. Bastianini, N. Galati, P. Casadei, and A. Nanni. 2005. *In-Situ Load Testing of Bridge A6358.* MoDOT.

Maurais, Daniel. 2012. *Strain Transfer of Notch Embedded Fiber Bragg Gratings.* Thesis, Laramie, WY: University of Wyoming.

Micron Optics (2010a). "Optical Strain Gage os3100." Web. 19 Mar. 2014.

Micron Optics (13 May 2014f). "Requirements and Considerations for Successful FBG Sensing Solutions." PowerPoint.

Mohammad, N., W. Syszkowski, W. Zhang, E. Haddad, J. Zou, W. Jamroz, et al. (2004). Analysis and Development of a Tunable Fiber Bragg Grating Based on Axial Tension/Compression. Journal of Lightwave Technology.

Pak, E. (1992). Longitudinal shear transfer in fiber optic sensors. Smart Mater. Struct., 1, 57-62.

Rivera, E., D. J. Thomson, and A. A. Mufti (2005). "Comparison of Recoated Fiber Bragg Grating Sensors under Tension on a Steel Coupon." *Nondestructive Evaluation and Health Monitoring of Aerospace Materials, Composites, and Civil Infrastructure IV* 5767.1: 163-74.

Seo, Junwon, Brent M. Phares, Ping Lu, Terry J. Wipf, and Justin Dahlberg (2012). "Use of a Structural Health Monitoring System for the Assessment of Bridge Load Rating." *Forensic Engineering 2012*: 18-27.

Tennyson, R.C., A.A. Mufti, S. Rizkalla, G. Tadros, and B. Benmokrane (2001). "Structural Health Monitoring of Innovative Bridges in Canada with Fiber Optic Sensors." *Smart Materials and Structures* 10: 560-73.

Todd, M, C. Chang, G. Johnson, S. Vohra, J. Pate, and R. Idriss. 1999. "Bridge Monitoring Using a 64-Channel Fiber Bragg Grating System." *17th International Modal Analysis Conference.* Kissimmee, FL: Society for Experimental Mechanics. 1719-1725.

Torres, B., I. Paya-Zaforteza, P. Caldron, P., and J. Adam. (2010). "Analysis of the strain transfer in a new FBG sensor for Structural Health Monitoring." *Engineering Structures*, 539-548.

Zhou, Zhi, and Jinping Ou. 2004. "Development of FBG Sensors for Structural Health Monitoring in Civil Infrastructures." *Sensing Issues in Civil Structural Health Monitoring.* Oahu: North American Euro-Pacific Workshop.

Zhou, J., Z. Zhou, and D. Zhang. (2010). "Study on Strain Transfer Characteristics of Fiber Bragg Grating Sensors." *Intelligent Material Systems and Structures*, 1117-1122.

Zhou, Zhi et al. (20 July 2015). "The Application of FBG Sensing in Monitoring Hulanhe Bridge in Heilong Jiang Province." Micron Optics.